


รายงานวิจัยฉบับสมบูรณ์

โครงการ การออกแบบอุปกรณ์ตรวจจับแก๊สแบบใหม่ซึ่งใช้ซิลิซีน

Title A new gas sensor design based on silicene

โดย ดร.จริญาณี ประสงค์กิจ และ คณะ

กรกฎาคม 2558

สัญญาเลขที่ 5680186

รายงานวิจัยฉบับสมบูรณ์

โครงการ การออกแบบอุปกรณ์ตรวจจับแก๊สแบบใหม่ซึ่งใช้ซิลิซีน

Title A new gas sensor design based on silicene

ผู้วิจัย	สังกัด
1. ดร. จริญาณี ประสงค์กิจ	คณะวิทยาศาสตร์ มหาวิทยาลัยนครพนม
2. รศ. ดร. วิทยา อมรกิจบำรุง	คณะวิทยาศาสตร์ มหาวิทยาลัยขอนแก่น

สนับสนุนโดยสำนักงานกองทุนสนับสนุนการวิจัย สำนักงานกองทุนสนับสนุนการวิจัย และมหาวิทยาลัยนครพนม

บทคัดย่อ

รหัสโครงการ : MRG5680186
ชื่อโครงการ : การออกแบบอุปกรณ์ตรวจจับแก๊สแบบใหม่ซึ่งใช้ซิลิซีน
ชื่อนักวิจัย : ดร. จริญาณี ประสงค์กิจ
E-mail Address : jariyanee.prasongkit.npu.ac.th
ระยะเวลาโครงการ : กรกฎาคม 2556 - กรกฎาคม 2558

การตรวจวัดชนิดของแก๊สในสิ่งแวดล้อมหรือการรั่วไหลของแก๊สในงานอันตรายเป็นความน่ากังวลอย่างใหญ่หลวงซึ่งเกี่ยวพันต่อสุขภาพ ความปลอดภัย และ ความเสี่ยงด้านสิ่งแวดล้อม ในความพยายามที่จะพัฒนาความสามารถในการตรวจจับแก๊ส วัสดุนาโนได้ถูกพิจารณาในฐานะเครื่องมืออันเป็นความหวังที่จะเอาชนะปัจจัยที่จำกัดหลักๆของเทคโนโลยีแก๊สเซ็นเซอร์ อันได้แก่ ความจำเพาะ ความไว เวลาตอบสนอง และ ความเสถียร เป็นต้น ความก้าวหน้าในการสร้างซิลิซีนได้ยกระดับความหวังอันน่าตื่นเต้นสำหรับการประยุกต์ใช้ในเชิงปฏิบัติสำหรับการตรวจจับแก๊ส โครงการวิจัยนี้ได้ศึกษาความสามารถในการตรวจจับแก๊สของนาโนเซ็นเซอร์ซิลิซีน สำหรับแก๊สที่แตกต่างกัน 4 ชนิด ได้แก่ NO, NO_2, NH_3 และ CO ในเทอมของความจำเพาะและความไว ซึ่งใช้ทฤษฎีฟังก์ชันนัลความหนาแน่นและวิธีกรีนฟังก์ชันไม่สมดุล สัญฐานเชิงโครงสร้าง ตำแหน่งการดูดซับ พลังงานยึดเหนี่ยว และการถ่ายโอนประจุของโมเลกุลแก๊สทั้งหมดที่ถูกศึกษาบนนาโนเซนเซอร์ซิลิซีนได้ถูกอภิปรายอย่างเป็นระบบ ผลการคำนวณชี้ให้เห็นว่า ซิลิซีนบริสุทธิ์แสดงความไวอย่างมากสำหรับแก๊ส NO และ NO_2 ขณะที่ไม่สามารถตรวจจับแก๊ส CO และ NH_3 ได้ ในความพยายามที่จะเอาชนะข้อจำกัดในด้านความไวอันเป็นผลจากอันตรกริยาแวนเดอร์วาลส์อย่างอ่อนของแก๊ส CO และ NH_3 บนอุปกรณ์ เราได้ทำการโด๊ปซิลิซีนด้วย B และ N ซึ่งนำมาสู่การเพิ่มขึ้นของพลังงานยึดเหนี่ยวและการถ่ายประจุและเป็นผลให้อุปกรณ์มีความไวที่ดีขึ้น อุปกรณ์ซิลิซีนแสดงความเป็นไปได้ในการแยกความต่างระหว่างแก๊สที่ถูกศึกษาทั้งสี่ชนิด จึงเป็นความหวังของนาโนเซ็นเซอร์ยุคถัดไปสำหรับการเป็นอุปกรณ์ตรวจจับแก๊สที่ความไวและความจำเพาะสูง

คำหลัก : ซิลิซีน อุปกรณ์นาโน ทฤษฎีฟังก์ชันนัลความหนาแน่น แก๊สเซนเซอร์

Abstract

Project Code : MRG5680186
Project Title : A new gas sensor design based on silicene
Investigator : Dr. Jariyanee Prasongkit
E-mail Address : jariyanee.prasongkit.npu.ac.th
Project Period : July 2556 - July 2558

Detection of chemical species in environment or gas leak in hazardous work is of a great concern as it involves health, safety and environmental risks. In an attempt to improve gas sensing performance, nanomaterials are being considered as a promising tool to overcome the main limiting factor of gas sensor technology; selectivity and sensitivity, response time and stability. Recent advances in the fabrication of silicene devices have raised exciting prospects for practical applications such as gas sensing. We investigated the gas detection performance of silicene nanosensors for four different gases (NO, NO_2, NH_3 and CO) in terms of sensitivity and selectivity, employing density functional theory and non-equilibrium Green's function method. The structural congurations, adsorption sites, binding energies and charge transfer of all studied gas molecules on silicene nanosensors are systematically discussed in this work. Our results indicate that pristine silicene exhibits strong sensitivity for NO and NO_2, while it appears incapable of sensing CO and NH3. In an attempt to overcome sensitivity limitations due to weak van der Waals interaction of those latter gas molecules on the device, we doped pristine silicene with either B or N atoms, leading to enhanced binding energy as well as charge transfer, and subsequently a signicant improvement of sensitivity. A distinction between the four studied gases based on the silicene devices appear possible, and thus promising to be next-generation nanosensors for highly sensitive and selective gas detection.

Keywords : Silicene, Nanodevices, Density Functional Theory, Gas sensor

Contents

List of Figures

List of Tables

CHAPTER I

Introduction

In today's world, there exist various kinds of threats in the form of dangerous gases or chemicals. These threats are serious problem, which can cause many long-term chronic health effects, particularly to people living around industrial areas [1,2]. Thus, the possibility for detection of gas leaks in a hazardous work environment has now become a fundamental issue involving safety, environmental and health risk. To keep the society safe, we need an effective gas sensor which is able to detect one atom/molecule of the gas. We believe nowadays that the potentials of nanotechnology become a promising way to overcome the limiting factor of gas sensors in improving selectivity and sensitivity and response time.

Two-dimensional nanostructure materials have taken the front row in innovative applications in the last decade after the successful experimental exfoliation of graphene. Gas sensors based on graphene have attracted much attention since graphene has excellent sensitivity to detect various gas molecules, large sensing area per unit volume, low electronic temperature noise, fast response time and high chemical stability [3,4]. The potential use of graphene for gas detection has been intensively investigated both experimentally [5-6] and theoretically [8-10]. However, growth of graphene over large surface areas is constrained. This motivated the search for other materials with similar favorable properties. In turn, this has led to the discovery of silicene as a silicon counterpart. The good properties with versatile silicon based nanotechnology gives the edge to silicene rather than graphene. This serves as the motivation of our work to theoretically explore the applicability of silicene for gas sensing.

The massless Dirac Fermions are the main reasons behind the ultrahigh carrier mobility for both the honeycomb structures of silicene and graphene [11-12]. Geometrically, the hexagonal structure of silicene has a larger size due to the larger ionic radius of Si atoms [13], but they have similar electronic structures. One important demarcation between the two structures is a buckled formation in silicene. This is due to sp^3 and sp^2 hybridization [14] rather than only sp^2 hybridization. This feature leads to a few prominent differences in the properties of silicene and graphene. Band gap tuning with an external electric field [15-17] and with the binding adsorbates [18-20] can be seen more profoundly in silicene than in graphene [21]. Although free-standing silicene has not been achieved so far, recent progress shows that it can be synthesized experimentally by depositing silicon on different surfaces such as silver [22] gold [23], zirconium diboride [24] and iridium [25].

To date, a wide range of potential applications of silicene have been proposed in various field such as spintronics [26-28], FETs [29-31], hydrogen storage [32,33] and sensing devices [34,35]. Nevertheless, using silicene as gas sensor has not been given the attention it deserves. Two theoretical investigations based on the density functional theory (DFT) were done to explore potential application of silicene as a molecular sensor for gas molecules [36,37]. They revealed changes in the electronic structures of silicene with adsorbed gas. The prime parameters to characterize the sensor performance of a gas sensor are sensitivity, selectivity, response time and recovery time. They should be addressed simultaneously to meet real application requirements of silicene based sensing systems.

The purpose of our study was therefore twofold. Firstly, we used the state-of-the-art first-principle methods to study the electronic and transport properties to evaluate the gas discrimination of silicene in terms of sensitivity and selectivity. Secondly, we demonstrate the possibility to improve gas sensing performance of silicene through doping this material with B and N atoms.

In this work, we investigated the electronic and transport properties of gas molecules adsorbed onto pristine (P) and B/N-doped silicene by employing a robust combination of non-equilibrium Green's function (NEGF) techniques and DFT. Four representative gas species; i.e., NO_2, NO, NH_3 and CO molecules, which are of main interest for environmental safety and medical purposes, were shown to be detectable by silicene based sensor devices. The sensitivity and selectivity of the devices to the presence of those gas molecules were evaluated from the changes in their electronic transport properties. Our results indicate that doping impurity atoms into silicene can enhance the interaction between the gas molecules and doped devices. This enabled an immense improvement in the performance of this type of sensor.

CHAPTER II
Research Methodology

In this chapter, we will give a theoretical background of the density functional theory (DFT), used for the electronic structure calculations in this thesis. Here, our aim is to provide to the reader a brief overview of the theory. Details of DFT can be found in many books and review articles [38-42]. At the end of this chapter, we describe how we can calculate electronic structures based on DFT.

2.1 Density Functional Theory

2.1.1 The many body problem

Well-defined collection of atoms forming molecules, solids, gases, liguids, etc. composes of electrons and nuclei. With quantum mechanics, we can describe a system of interacting electrons and nuclei by solving the Schrödinger equation

$$\hat{H}\Psi = E\Psi, \tag{2.1}$$

where E is the energy eigenvalue and the many-body hamiltonian operator is

$$\hat{H} = \sum_{i=1}^{N_e} -\frac{\hbar^2}{2m}\nabla_i^2 + \sum_{I=1}^{N_{nuc}} -\frac{\hbar^2}{2M}\nabla_I^2 + \frac{1}{2}\sum_{i\neq j}\frac{e^2}{|\mathbf{r}_i - \mathbf{r}_j|} \tag{2.2}$$
$$-\sum_{i,I}\frac{Z_I e^2}{|\mathbf{r}_i - \mathbf{R}_I|} + \frac{1}{2}\sum_{I\neq J}\frac{Z_I Z_J e^2}{|\mathbf{R}_I - \mathbf{R}_J|}$$

In the Eq. (2.2), the first and second terms are the kinetic energy of electrons and nuclei, and the last three terms are the electron-electron interactions, electron-nucleus interactions and nucleus-nucleus interactions, respectively. $\hbar$ is planck's constant, *m* and *M* are electron and nucleus mass, respectively. Z_I is the atomic number of the I^{th} atom, *e* is the electron charge, $\mathbf{r}_i$ and $\mathbf{R}_I$ are the positions of the electron i^{th} and I^{th} nucleus.

Solving the many-body Schrödinger equation is a very complicated many-body problem. To simplify the problem, Born-Oppenheimer approximation is used,

stating that the nuclei are much heavier than the electrons and they move much more slowly than electrons can. As a result, we can split the electronic and nuclear motions. The nuclei positions are treated as fixed while the electrons are moving in the field of charged nuclei. The total wave function is separated into electronic and ionic wave functions. Consequently, the Schrödinger equation can be written for electronic part as

$$\hat{H}_e(\mathbf{r}, \mathbf{R})\Psi_e = E_e\Psi_e(\mathbf{r}, \mathbf{R}), \tag{2.3}$$

with the electronic Hamiltonian given by

$$\hat{H} = \sum_{i=1}^{N_e} -\frac{\hbar^2}{2m}\nabla_i^2 + \frac{1}{2}\sum_{i\neq j}\frac{e^2}{|\mathbf{r}_i - \mathbf{r}_j|} + \hat{V}_{ext} \tag{2.4}$$

where $\hat{V}_{ext}$ is the potential acting on the electrons due to the nuclei. Note that the interaction between nuclei enters as a constant parameter. Although the number of degrees of freedom of the system can be reduced by using Born-Oppenheimer approximation, solving the problem of the electron-electron interaction is still difficult to solve. Moreover, the electronic wave function depends on all electron coordinates, where the number of electrons is considerably larger than the number of nuclei. As it will be shown in a moment, it is more practical to use density functional description instead of the many-body wave functions. DFT requires less consuming computational effort, and gives a good description for ground state properties of electronic systems.

2.1.2 The Hohenberg-Kohn theorems

The main idea of DFT is to describe the interacting system via the electron density instead of the many-body wave functions. DFT methods are founded on two fundamental theorems by Hohenberg and Kohn [43]. The first theorem is: *The ground state energy of a system of interacting electrons is a unique functional of the electronic charge density*. In other words, there exists a one-to-one correspondence between the ground-state wave function and the ground-state electron density.

The first Hohenberg-Kohn theorem only gives a proof of the existence of a functional of electron density, which can be used to solve the Schrödinger equation, however, its true functional form is unknown. The second Hohenberg-Khon theorem, defining the property of the functional, is: *The electron density that minimizes the energy of the overall functional is the true ground-state electron density*.

According to these theorems, the expectation value of the Hamiltonian in Eq. (2.4) can be expressed as

$$< \psi|\hat{H}|\psi >= E[n(\mathbf{r})], \tag{2.5}$$

where $E[n(\mathbf{r})]$ is the total energy functional and $n(\mathbf{r})$ is the electron density. Therefore, if we know the energy functional form, we can vary the electron density until the energy functional is minimized by using the variational principle

$$\left.\frac{\delta E[n(\mathbf{r})]}{\delta n}\right|_{n=n_0} = 0. \tag{2.6}$$

According to the second theorem, the density corresponding to the minimum energy $(E_0)$is the ground-state density, $n_0(\mathbf{r})$. However the view of the first theorem, there is only one ground-state wave function ψ_0 , corresponding to $n_0(\mathbf{r})$, and therefore only one ground-state energy, which is

$$E_0 =< \psi_0|\hat{H}|\psi_0 >= E[n_0(\mathbf{r})]. \tag{2.7}$$

2.1.3 Kohn-Sham equations

Kohn and Sham [44] proposed a way to reduce the original many-body problem into an auxiliary one-electron problem. The way is to replace interacting electrons into a non-interacting electron moving in an effective potential. The total energy functional in Eq. (5) can be written as

$$E[n(\mathbf{r})] = T_0[n(\mathbf{r})] + \frac{1}{2}\int\int \frac{n(\mathbf{r})n(\mathbf{r}')}{|\mathbf{r}-\mathbf{r}'|}d\mathbf{r}d\mathbf{r}' + \int V_{ext}(\mathbf{r})n(\mathbf{r})d\mathbf{r} + E_{xc}[n(\mathbf{r})], \tag{2.8}$$

where $T_0[n(\mathbf{r})]$ is the kinetic energy functional of the non-interacting electron system, the second term is the electrostatic energy or Hartree energy, the third term is the external energy due to the nuclei and the last term is all the remaining contribution to the energy, called the exchange and correlation energy.

By minimizing of Eq.(2.6) with respect to the density, we get the single-particle Kohn-Sham equations:

$$\left[-\frac{\nabla_i^2}{2} + V_{eff}(\mathbf{r})\right]\Psi_i(\mathbf{r}) = \epsilon_i\Psi_i(\mathbf{r}), \tag{2.9}$$

where

$$V_{eff}(\mathbf{r}) = V_{ext} + \int \frac{n(\mathbf{r}')}{|\mathbf{r}-\mathbf{r}'|}\,d\mathbf{r} + \frac{\delta E_{xc}[n(\mathbf{r})]}{\delta n(\mathbf{r})}.$$

Note that the Kohn-Sham wave functions, $\Psi_i(\mathbf{r})$ do not give any direct physical meaning. They are just auxiliary functions for calculating the electron density. The electron density can be obtained from the Kohn-Sham wave functions,

$$n(\mathbf{r}) = \sum_{i=1}^{N} |\Psi_i(\mathbf{r})|^2. \qquad (2.10)$$

In order to find the ground-state electron density, the Khon-Sham equations have to be solved self-consistently by iterative methods with the following algorithm:

1. Define an initial guess of electron density,
2. Solve the Kohn-Sham equations to get the Kohn-Sham wave functions, $\Psi_i(\mathbf{r})$
3. Calculate the electron density defined by the Kohn-Sahm wave functions from the step 2.
4. Compare the calculated electron density, with the electron density used in solving the single-particle Kohn-Sham equations. If two densities are the same, then we get the ground-state electron density, and it can be used to compute the energy, forces, stresses, etc. If the two densities are different, the process begins again from the step 2.

2.1.4 Exchange-correlation functionals

Kohn-Sham scheme shows us how to transform the many-body problem into an effective single-electron problem. Only one challenge is that we must specify the exchange-correlation function , $E_{xc}[n(\mathbf{r})]$. Unfortunately, the exact form of the exchange-correlation functional is simply not known, hence the approximation has to be done.

The simplest approximation is the so-called local density approximation (LDA) [44], derived from the exchange-correlation energy of the homogeneous electron gas. The LDA exchange-correlation functional is written as

$$E_{xc}^{LDA}[n(\mathbf{r})] = \int n(\mathbf{r})\epsilon_{xc}^{hom} d\mathbf{r}, \qquad (2.11)$$

where ϵ_{xc}^{LDA} is the exchange-correlation energy density of a homogeneous electron gas with the electron density, $n(\mathbf{r})$. Thus, the only information required is the exchange-correlation energy of the homogeneous electron gas, which can be derived exactly. Since the functional derived from locally uniform electron gas, the error would be expected for quickly varying densities. The LDA works very well for bulk solids. However

it is necessary to use other functionals if the electron densities are not slowly varying, for instance, in atoms and molecules.

A generalized gradient approximation (GGA), the best known functional developed after the LDA, has also included the local gradient of the electron density, $\nabla n(\mathbf{r})$. There are many attempts to find a good functional form, two of the most commonly used functionals are the Perdew-Wang functional (PW91) [45] and the Perdew-Burke-Ernzerhof (PBE) [46]. In general, it is assumed that the GGA should provide more accurate results than the LDA, because it includes more physical ingredient i.e., gradient of density. This is not always true. In some cases, the results of LDA are better than that of the GGA when compared with experiments [47,48].

2.1.5 Computational methods

So far, we have not described how to calculate electronic structures based on DFT methods. The SIESTA (Spanish Initiative for Electronic Simulations with Thousands of Atoms) code [49] has been chosen as the main tool for electronic structure calculation, since the transport codes used in this thesis are TranSIESTA [49] and SMEAGOL [50,51], based on SIESTA code. The computational methods, used in solving Kohn-Sham equations with SIESTA code, will be briefly described in this section.

2.1.5.1 Bloch's theorem and basis sets

To solve Kohn-Sham Eq. (2.6), the appropriate boundary conditions need to be specified. The SIESTA code has used periodic boundary condition to simulate a supercell with replicating a unit cell in all the three dimensions. This is convenient for the infinite and periodic systems such as the bulk crystal. It can also be used for the finite system such as a molecular species, where the molecule is placed in a sufficiently large unit cell in order to avoid the interaction with its own image. By using the supercell approach according to the Bloch's theorem [52], the Kohn-Sham wave function can be written as a product of a wavelike part and a cell-periodic part, i.e.,

$$\Psi_{\mathbf{k}}^{n}(r) = u_{\mathbf{k}}^{n}(r)e^{i\mathbf{k}\cdot\mathbf{r}}, \qquad (2.12)$$

where *n* is a discrete band index and $\mathbf{k}$ is a vector in the reciprocal space. This theorem means that it is possible to map Khon-Sham equation into the reciprocal space, and solve the equation for each value of $\mathbf{k}$ independently.

Choosing an appropriate basis is necessary to obtain accurate results. One possible choice of basis set is a plane wave. For the periodic systems, the plane wave basis sets appear to be the natural choice. The advantages of plane wave basis set are

the simplicity of basis function, where the fast Fourier transform algorithm can be efficiently made, the absence of basis set superposition error, and the ability to control accuracy with increasing the number of waves.

However, solving the Kohn-Sham equations using plane wave as a basis set is computationally demanding due to the large number of plane waves needed in order to describe localized states. The plane waves are not centered at the nuclei but extend over all space. They also propagate across the whole cell, even when there is no charge density, and is therefore unsuitable for grid-based electronic structure calculation for large systems.

In SIESTA, solving the Kohn-Sham equation uses linear combination of localized numerical atomic orbitals (LCAO) as a basis set. It can be written as products of a radial function multiplied and spherical harmonics

$$\phi_{lmn}(r,\theta,\varphi) = R_{n,l}(r)Y_{l,m}(\theta,\varphi), \qquad (2.13)$$

where $R_{n,l}$ and $Y_{l,m}$ are radial function for orbital n and real spherical harmonic for orbital angular momentum l and magnetic quantum number m, respectively. The radial function becomes zero beyond a certain radius.

Unlike plane waves, the basis sizes and shape must be chosen for the given system to obtain the accurate results. One can expand the number of basis functions using a multiple- basis set. Each ζ orbital corresponds to the same spherical harmonics but with different radial functions, i.e. single- ζ or ``SZ'', double- $\zeta$ or ``DZ'', triple- ζ or ``TZ'' for 1, 2 or 3 radial functions, etc. Moreover, it is possible to include polarization functions, to account for the deformation induced by the bond formation in molecules or solids. The polarization function has an angular momentum one unit higher than the maximum occupied state in the atom; i.e. the p-orbitals can be used for polarizing s-orbitals, likewise, d-orbitals can be used for polarizing p-orbitals, etc. Adding polarization functions in the basis is denoted by ``P'', e.g. ``DZP'' for double ζ with polarization functions. The quality of basis sets can be checked by comparing energies and geometries at different levels, but DZP generally provides high-quality results with a reasonable computational cost for most of the systems.

2.1.5.2 Pseudopotential

Solving the Kohn-Sham equation can be simplified if we can decrease the computational burden due to core electrons. Since the strong Coulomb potential and tightly bound core electrons in atoms are associated with rapidly varying wave functions with many nodes, it is necessary to use a large number of basis functions to describe

them. However, the core electrons do not play a significant role to define chemical bonding or other varying physical properties; these properties are described by valence electrons. As a result, we can replace the strong Coulomb potential of the nucleus and the effects of tightly bound core electrons by pseudopotential, which still keeps various important physical and mathematical properties of the true ion core. The pseudo wave functions have to coincide with the all-electron wave function beyond the core radius, r_c, and the pseudo wave functions are forced to have the same norm as the all-electron valence wave functions;

$$R_l^{PP}(r) = R_{nl}^{AE}(r) \qquad \text{, if } r > r_c$$
$$\int_0^{r_c} dr|R_l^{PP}|^2 r^2 = \int_0^{r_c} dr|R_{nl}^{AE}(r)|^2 r^2 \qquad \text{, if } r < r_c \tag{2.14}$$

where $R_l(r)$ the radial part of the wave function with angular momentum l. PP and AE denote the pseudo wave function and the all-electron wave function. The index n is the valence level of all-electron wave function.

There are two other conditions that the pseudo wave functions should satisfy: it should have nodeless surfaces and the pseudo energy eigenvalues should match the all-electron eigenvalues. The pseudopotential constructed in this way is called norm-conserving pseudopotential. In SIESTA, one generally uses norm-conserving pseudopotentials according to the Troullier-Martins parameterization [53], based on earlier work by Kerker [54].

2.2 Quantum transport theory

2.2.1 Transport regimes

In the field of electron transport in mesoscopic and nanoscopic systems, there are different approaches that have been used for each transport regime. Before setting up the transport calculation, therefore, we need to define the transport regime for given problems. Two characteristic lengths used to distinguish the transport regime are the momentum relaxation length, L_m , and the phase relaxation length, L_ϕ. The momentum relaxation length (or electron mean free path) is the average distance travelled by electrons until their momentum relax, while the phase relaxation length is the average distance travelled by electrons until their phase relax.

If the length of the device, L , is much longer than L_m and L_ϕ , the conductance is dependent on the length of the wire obeying the simple Ohm's law. That is the reason we called it as ohmic regime.

The development of electronic devices at the single-molecule scale has expanded existing theories of electrical transport beyond their limits. Due to the small size of such a device, the quantum character of the electrons is considered since electrons act like waves showing interference effects. Under two characteristic lengths, we can divide electron transport into three transport regimes:

(1) Ballistic transport regime, $\mathbf{L} << \mathbf{L_m}, \mathbf{L}_\phi$

There is no significant momentum and phase relaxation in the electron transport process through a device. Electrons can propagate freely, meaning that the resistance can arise from only the contact region. Ballistic conduction is typically observed in quasi-1D structures, such as carbon nanotubes or metallic nanowires, with quantized conductance ($G_0 = 2e^2/h$, where e is the electron charge and h is the Plank constant). The conductance of such a device is independent of its length.

(2) Elastic and coherent transport regime, $\mathbf{L} < \mathbf{L_m}, \mathbf{L}_\phi$

The incoherent transport regime can be generally observed in a long molecular bridge. Since the long traverse time of electrons, they can interact with other electrons or phonon that would constitute a phase-breaking or incoherent scattering process. As a result, the phase of the electron waves is lost in addition to the change of the electron momentum. The dynamic of the molecular chain plays a significant role in the transmission instead of the contact region.

(3) Inelastic and incoherent transport regime, $\mathbf{L} \geq \mathbf{L_m}, \mathbf{L}_\phi$

The incoherent transport regime can be generally observed in a long molecular bridge. Since the long traverse time of electrons, they can interact with other electrons or phonon that would constitute a phase-breaking or incoherent scattering process. As a result, the phase of the electron waves is lost in addition to the change of the electron momentum. The dynamic of the molecular chain plays a significant role in the transmission instead of the contact region.

There are two approaches that have been widely used to study the transport problem: the Landauer method and the Non-Equilibrium Green's Function (NEGF) method. The Landauer approach allows us to describe the non-interacting electron transport corresponding to the ballistic or elastic transport regimes, while the NEGF approach is a more sophisticated method that can be used in all three transport regimes. In the following sections, we will briefly describe the computational

implementation based on Landauer and NEGF method for elastic transport regime, related to the transport problem in this research.

2.2.2 Landauer approach

In the Landauer approach, we can imagine for a system of two macroscopic electrodes connecting to the molecule or nanoscale structure. The system comprises the three regions: left (L) and right (R) leads and a central region (C). The two leads are connected to electron reservoirs, and kept at two different electrochemical potential, μ_L and μ_R , where $\mu_L = \mu_R$ at zero applied voltage. The electric current will flow when the voltage is applied.

In a such geometry, the problem can be viewed as a scattering problem: an incident wave function propagating along the central region and scattered by a potential connecting to the two leads and then transmitted to the other lead. Landauer viewed the current flow as the probability of the electron to be transmitted from one lead to the other. Here, we will present the simple way to derive the Landauer formula, but still show the important concept related to computational implementations. The rigorous derivation of this approach can be found in Ref.55.

Let us consider an ideal one-dimensional wire of length L between two leads. This system is assumed to be the ballistic transport regime. In the wire, states in the direction normal to the propagation are quantized. The density of state corresponding to the given perpendicular state in the momentum range between k and $k + dk$, including spin is

$$n(k)dk = 2\frac{1}{L}\frac{L}{2\pi}dk = 2\frac{1}{2\pi}f(k)dk, \qquad (2.15)$$

where $f(k)$ is the Fermi distribution function.

When the voltage is applied, the leads are in the equilibrium, where the Fermi distribution functions for the left and the right lead are $f_L(k)$ and $f_R(k)$, respectively. The current flow through such a system is

$$I = 2\int_0^\infty ev(k)n(k)dk = 2\int_0^\infty e\frac{\hbar k}{m_e}\left(\frac{f_L(k)}{2\pi} - \frac{f_R(k)}{2\pi}\right)dk \qquad (2.16)$$

where $v(k)$ is the electron velocity along the wire and m_e is the electron effective mass. At the zero temperature, the Fermi distributions are step functions, and Eq. (2.16) becomes

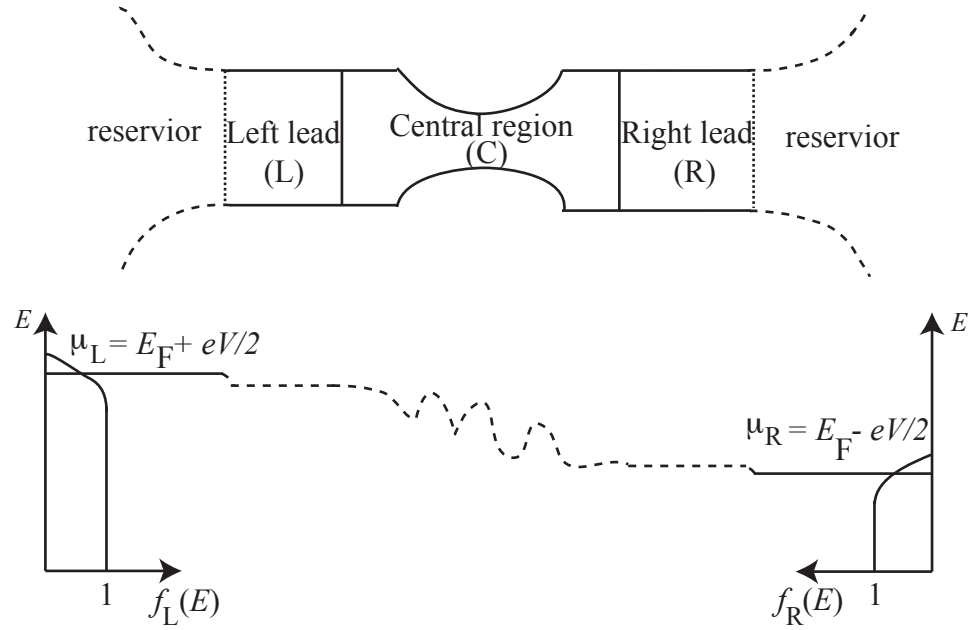

Figure 2.1: The setup of the Landauer approach: the left and right leads (L,R) are connected to two reservoirs in equilibrium at two different electrochemical potentials (μ_L, μ_R). Both leads are connected to the central region (C), in which scattering can take place. The electrochemical potential is almost flat inside the leads and the potential drop occurs across the junction.

$$I = 2\int_{\sqrt{2m_e\mu_R}/\hbar}^{\sqrt{2m_e\mu_L}/\hbar} e\frac{\hbar k}{m_e}\frac{1}{2\pi}dk = 2\frac{e^2}{h}\frac{\mu_L - \mu_R}{e} = 2\frac{e^2}{h}V_B, \quad (2.17)$$

where μ_L and μ_R are the electrochemical potential of left and right lead, respectively. V_B is the bias voltage due to the shift of electrochemical potential of both leads; $\mu_L - \mu_R = eV_B$.

The maximum conductance of a one conduction channel with two spin states, G_0, is thus,

$$G_0 = \frac{2e^2}{h} = (12.9k\Omega)^{-1}. \quad (2.18)$$

This is the so-called quantum of conductance. Generally, the nanodevice and its connection to the leads is not ideal due to scattering. Therefore, at low temperatures in the linear response regime, the formula for the conductance can be written as

$$G = \frac{2e^2}{h} T(E_F), \tag{2.19}$$

where E_F is the Fermi energy of the system. The Eq. (2.18) is for the one-dimensional wire, where there is only one conducting mode in the direction normal to the propagation. If we now allow for the finite width devices, the number of quantum modes carrying electrons are to be considered. The Landauer formula can be generalized to

$$G = \frac{2e^2}{h} \sum_{i,j} T_{ij}(E_F), \tag{2.20}$$

where T_{ij} is the probability of electrons passing from i^{th} conducting mode at the left of the device to the j^{th} conducting mode at the right of the device. More generally, the current at a finite bias can be expressed as

$$I = \int_0^\infty \frac{dE}{e} (f^L(E) - f^R(E)) G(E), \tag{2.21}$$

where $G(E)$ is defined in Eq. (2.20). According to Landauer formula, only one ingredient required is the energy dependent transmission function. This is typically derived from the Green's function of the central region coupling with both leads, as we will discuss in the following section.

2.2.3 Non-equilibrium Green functions (NEGF)

The study of electron transport is modelled on the atomic level, therefore, combining NEGF method with DFT has a great advantage over other methods. In this section, we will give the reader an understanding of the basic concepts of the NEGF method to calculate current-voltage characteristic of molecular devices.

We start from the screening approximation, dividing the system into lead and central regions, and then the Hamiltonian of the system is determined. By using the NEGF method, the charge density is calculated in a self-consistent manner. The section ends with a description on how one calculates the electron current with Landauer approach.

2.2.3.1 The screening Approximation

In the NEGF method, the setup is partitioned in the same way as in the Landauer method, where two semi-infinite leads, left (L) and right (R), are coupled with the central region (C) via a contact region. Fig. 2.2 illustrates the system setup. The semi-infinite leads have a regular periodic structure extending in the direction of the transport, consequently, the Hamiltonian of both leads has the infinite dimension. Using the screening approximation, we can divide the effective potential and charge density into the central region and lead regions, and the two leads are treated as bulk systems. The surface effects due to the perturbation of a molecule at the contact region, i.e. the charge transfer, atomic relaxation and the potential disturbance, are eliminated by including a few layer of leads to the central region.

Using the screening approximation, we can obtain the Hamiltonian matrix with the finite range, written as

$$\mathbf{H} = \begin{pmatrix} \mathbf{H}_{LL} & \mathbf{H}_{LC} & 0 \\ \mathbf{H}_{CL} & \mathbf{H}_{CC} & \mathbf{H}_{CR} \\ 0 & \mathbf{H}_{RC} & \mathbf{H}_{RR}, \end{pmatrix}, \qquad (2.22)$$

where $\mathbf{H_{LL}}$, $\mathbf{H_{CC}}$ and $\mathbf{H_{RR}}$ denote the Hamiltonian matrices of the left, central and right parts, respectively, and $\mathbf{H_{LC}}$ and $\mathbf{H_{CR}}$ are the matrices involving the central region and the leads. We assume that there is no direct tunneling between leads L and R.

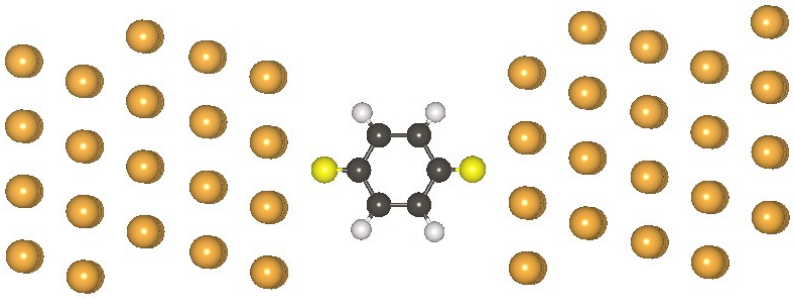

Figure 2.2: Schematic illustration of a system containing a molecule sandwiched between left (L) and right (R) leads.

The overlap matrix has the same structure as the Hamiltonian matrix:

$$\mathbf{S} = \begin{pmatrix} \mathbf{S}_{LL} & \mathbf{S}_{LC} & 0 \\ \mathbf{S}_{CL} & \mathbf{S}_{CC} & \mathbf{S}_{CR} \\ 0 & \mathbf{S}_{RC} & \mathbf{S}_{RR} \end{pmatrix}. \qquad (2.23)$$

After identifying the Hamiltonian and overlap matrices, the next step is to calculate the retarded Green's function to determine the charge density, described in the following section.

2.2.4 Calculating the charge density

Exploiting the NEGF formalism, we can write the whole system in the term of retarded Green's function

$$[\epsilon^{+}\mathbf{S} - \mathbf{H}]\mathbf{G}^{R}(E) = \mathbf{I}, \tag{2.24}$$

where $\epsilon^{+} = \lim_{\eta \to 0^{+}} E + i\eta, E$ is the energy, and $\mathbf{I}$ is an infinitely-dimensional identity matrix. By substituting the Eq.(2.22) and Eq.(2.23}) into Eq.(2.24), we obtain

$$\begin{pmatrix} \epsilon^{+}\mathbf{S}_{LL} - \mathbf{H}_{LL} & \epsilon^{+}\mathbf{S}_{LC} - \mathbf{H}_{LC} & 0 \\ \epsilon^{+}\mathbf{S}_{CL} - \mathbf{H}_{CL} & \epsilon^{+}\mathbf{S}_{CC} - \mathbf{H}_{CC} & \epsilon^{+}\mathbf{S}_{CR} - \mathbf{H}_{CR} \\ 0 & \epsilon^{+}\mathbf{S}_{RC} - \mathbf{H}_{RC} & \epsilon^{+}\mathbf{S}_{RR} - \mathbf{H}_{RR} \end{pmatrix} \begin{pmatrix} \mathbf{G}_{LL} & \mathbf{G}_{LC} & 0 \\ \mathbf{G}_{CL} & \mathbf{G}_{CC} & \mathbf{G}_{CR} \\ 0 & \mathbf{G}_{RC} & \mathbf{G}_{RR} \end{pmatrix}$$

$$= \begin{pmatrix} \mathbf{I}_{LL} & 0 & 0 \\ 0 & \mathbf{I}_{CC} & 0 \\ 0 & 0 & \mathbf{I}_{RR} \end{pmatrix} \tag{2.25}$$

In this problem, the central part directly interacts only with the finite part of the right and left leads. Therefore, we can focus on only the Green's function matrix of the central region and treat the effect of semi-infinite leads in the term of effective interaction. Then, the final expression for the retarded Green's function of the central region has the following form

$$\mathbf{G}^{R}_{CC}(E) = [\epsilon^{+}\mathbf{S}_{CC} - \mathbf{H}_{CC} - \mathbf{\Sigma}^{R}_{L}(E) - \mathbf{\Sigma}^{R}_{R}(E)], \tag{2.26}$$

where $\mathbf{\Sigma}^{R}_{L}(E)$ and $\mathbf{\Sigma}^{R}_{R}(E)$ are retarded self-energies of the left and right leads. The self-energies are associated to the energy level shift and energy level broadening, deriving from the real part $[\Delta_{L/R} = \mathrm{Re}\mathbf{\Sigma}_{L/R}]$ and the imaginary part $[\Gamma_{L/R} = -\mathrm{Im}\Sigma_{L/R}]$ of the self-energies, respectively, as shown in Fig. \ref{broaden}. Moreover, the broadening of the molecular levels is associated with the lifetime of the electronic states on the molecule. While the molecule is coupled to the leads, the electron can escape into

the right or left leads, and spend time in the state localized at the central region. The lifetime of state is inversely proportional to the broadening of electrons:$\tau_{L,R}\Gamma = \hbar$. We can also write the escape rates of electrons into the molecular level to the left(right) lead as $\Gamma_{L(R)}/\hbar$.

The self-energies of the left and right leads can be written in the form

$$\Sigma_L^R(E) = (\epsilon^+\mathbf{S}_{CL} - \mathbf{H}_{CL})\mathbf{G}_L^{0R}(\epsilon^+\mathbf{S}_{LC} - \mathbf{H}_{LC}) \qquad (2.27)$$

and

$$\mathbf{\Sigma_R^R}(\mathbf{E}) = (\epsilon^+\mathbf{S}_{CR} - \mathbf{H}_{CR})\mathbf{G}_R^{0R}(\epsilon^+\mathbf{S}_{RC} - \mathbf{H}_{RC}), \qquad (2.28)$$

where $\mathbf{G}_{L(R)}^{0R}$ is the retarded surface green function of the left(right) lead, defined by

$$\mathbf{G}_L^{0R} = [\epsilon^+\mathbf{S}_{LL} - \mathbf{H}_{LL}]^{-1} \qquad (2.29)$$

and

$$\mathbf{G}_R^{0R} = [\epsilon^+\mathbf{S}_{RR} - \mathbf{H}_{RR}]^{-1}. \qquad (2.30)$$

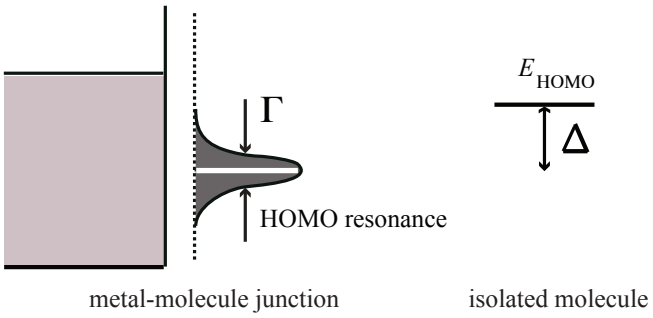

Figure 2.3: When the molecule is attached to semi-infinite leads, its energy levels are renormalized. The energy level broadening due to the coupling to the contact is given by **Γ**.

From Eq.(2.26)-(2.30) ,we can see that the retarded Green's Function describes the electronic structures and other properties of the central region connected to both leads. Clearly, infinite-dimensional Hamiltonian is reduced to the dimension of the central part where the self-energies, $\mathbf{\Sigma_L}$and$\mathbf{\Sigma_R}$, include all the information of the

semi-infinite properties of the leads. Thus, we can write the effective Hamiltonian associated to the retarded Green's function as

$$\mathbf{H_{eff}} = \mathbf{H_{CC}} + \mathbf{\Sigma_L^R} + \mathbf{\Sigma_R^R}. \tag{2.31}$$

The density matrix, $\mathbf{D}_{CC}$, is calculated by using the retarded Green's function

$$\mathbf{D}_{CC} = -\frac{1}{\pi}\mathrm{Im}\int_{-\infty}^{\infty}[\mathbf{G}_{CC}^{R}(E)f(E-\mu)]dE. \tag{2.32}$$

Then, the density matrix is used to calculate the electron density

$$\rho(\mathbf{r}) = \sum_{\alpha\beta}(\mathbf{D}_{CC})_{\alpha\beta}\phi_{\alpha}(\mathbf{r})\phi_{\beta}(\mathbf{r}), \tag{2.33}$$

where $\phi_{\alpha/\beta}$ is a localized atomic basis orbital.

In summary, to obtain the charge density, we need to combine NEGF formalism with DFT. The Hamiltonian is derived from the DFT procedure, and the charge the density for an open system is calculated with the NEGF technique. The retarded Green's function based on the Hamiltonian is defined, while the Hamiltonian is a functional of the electron density itself. The problem is usually treated in an iterative way as shown in Fig. 2.4

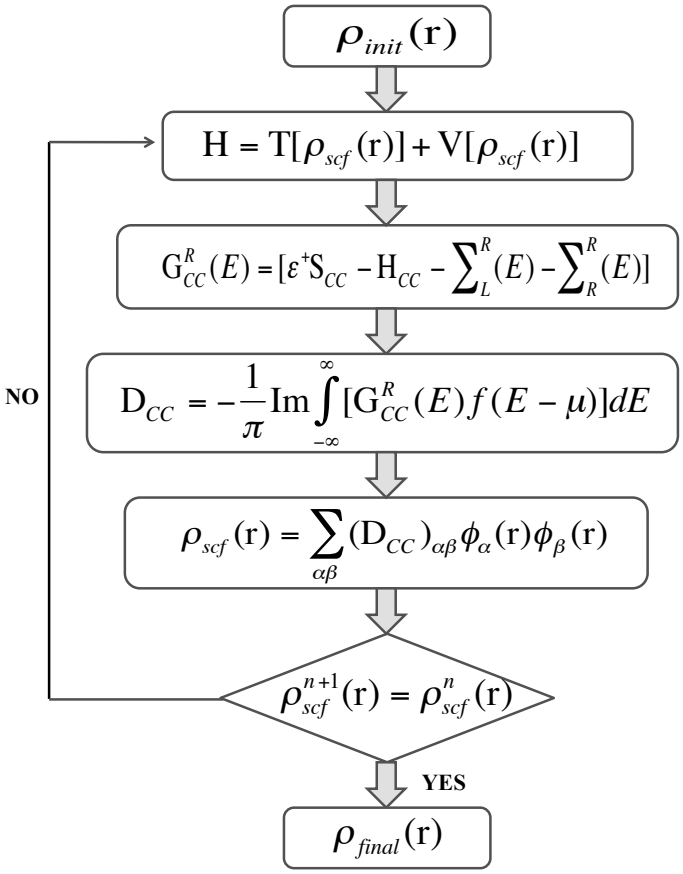

Figure 2.4: The schematic form of the self-consistency loop based on the NEGF+DGF method

CHAPTER III
Results and Discussion

This chapter concerns the first principle study on silicene gas sensors. Based on the DFT calculation, the geometrical structures of of gas molecules adsorbed onto pristine (P) and B/N-doped silicene were determined. The transport properties were calculated using the DFT-based non-equilibrium Green's function (NEGF) theory. This work allows us to investigate the gas detection performance of silicene nanosensors for four different gases. This chapter summarizes the study described in Paper I.

3.1 Geometric and Electronic structures

The geometrical structures of four different molecular gases (NO, NO_2, NH_3 and CO) adsorbed on pristine silicene and doped-silicene nanodevices were relaxed by using DFT [43,44] as implemented in the SIESTA package [49] To describe the weak dispersive interactions, we employed a van der Waals correction [56,57] to the Generalized Gradient Approximation of Perdew, Burke, and Ernzerhof (PBE-GGA) [46] for the exchange-correlation functional in DFT.

A description of van der Waals (vdW) were performed using vdW-DF, as proposed by Dion *et al.* [56]. In this methodology, the exchange-correlation energy is written as

$$E_{xc} = E_x^{GGA} + E_c^{LDA} + E_c^{nl}, \qquad (3.1)$$

where the exchange energy E_x^{GGA} uses the GGA functional, and E_c^{LDA} is the local density approximation (LDA) to correlation energy. The nonlocal correlation-energy part, E_c^{nl}, is defined to include the longest-ranged or most nonlocal energy term which is zero for systems with constant density.

For the ionic relaxation $6 \times 1 \times 4$ *k*-points and for the electronic transport $24 \times 1 \times 1$ *k*-points were used. Furthermore, double-ζ polarized basis sets (DZP) and norm-conserving pseudo potentials [53] were used. The conjugate gradient (CG) method was applied to obtain equilibrium structures with residual forces on atoms below 0.01

eV/$\mathring{A}$. We also employed VASP [code, using the same parameters as in of SIESTA for the relaxation and binding energy calculations with a 400 eV cutoff energy for the plane wave basis and a force tolerance of 0.01 eV/$\mathring{A}$. Silicene has a buckled hexagonal lattice, consisting of 2 Si atoms per unit cell. For transport calculation, each simulated system consisted of $20.57\mathring{A} \times 15\mathring{A} \times 43.54\mathring{A}$ silicene supercell with 132 Si atoms. We use the periodic boundary condition (PBC) along x-direction and z-direction and considerably large supercell to avoid the interaction occurring between mirror images. The neighboring silicene in y-direction was separated by $15\mathring{A}$ of vacuum. Details on supercell construction is presented in Figure 3.1. Silicene has a hexagonal lattice with two atoms per unit cell (A and B) as is shown in Figure 3.1-a. However, is also possible define an unit cell with four atoms and parallepiped shape (see Figure 3.1-b), in which the lattice is characterized by three lattice vectors L_x, L_y and L_z In particular both unit cells are equivalent, but as we are interested in L_z transport properties through the device in certain direction, the parallelepiped unit cell fits better for this application. In all calculation were employed a supercell using a parellepiped unit cell with $3L_x \times L_y \times 11L_z$ and 132 atoms as is shown in Figure 3.1-c. The referred supercell has $20.57\mathring{A} \times 15\mathring{A} \times 43.54\mathring{A}$.

The transport properties were then investigated with the TranSiesta code [58], combining the NEGF method and DFT. This was done to perform electronic transport calculations in order to visualize the degree of capability of pristine silicene and doped-silicene nanodevices as an electric nanosensors to distinguish four different molecular gases (NO, NO_2, NH_3, and CO). The basis sets and the real-space grid employed in the transport calculations are identical to those described above for the geometrical optimization part. The system was divided into three parts: two leads (left and right) and a scattering region in between them. The left panel of Figure 3.2 shows upper (pristine) and lower panel (doped) hexagonal 2D silicene that was used as a molecular gas sensor. The red shaded rectangles represent the electrodes or leads (left/right) and the region in between was the scattering region. Nitrogen (N) and boron (B) are the two substituted atoms used to functionalize silicene.

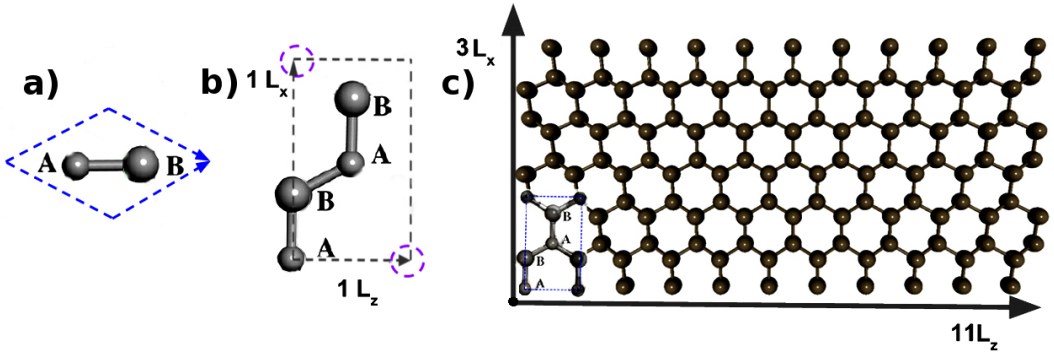

Figure 3.1: a) Hexagonal 2D lattice with two atoms per unit cell for silicene; b) A parallelepiped unit cell with four atoms per unit cell and (c) supercell used in relaxations and also transport calculation.

Defining the boundary as a region, where the charge density matches with the bulk electrodes and using localized basis sets, the NEGF for the scattering region $\mathcal{G}(E,V)$ can be formulated as following:

$$\mathcal{G}(E,V) = [E \times S_{\mathrm{S}} - H_{\mathrm{S}}[\rho] - \Sigma_{\mathrm{L}}(E,V) - \Sigma_{\mathrm{R}}(E,V)]^{-1}$$

where S_S and H_S are the overlap matrix and the Hamiltonian, respectively, for the scattering region. $\Sigma_{L/R}$ are self-energies that account for the effect from the left (L) and right (R) electrodes upon the central region. The self energies are given by, $\Sigma_\alpha = V_{S\alpha} g_\alpha V_{\alpha S}$, where g_α are the surface Green's functions for the semi-infinite leads and $V_{\alpha S} = V_{S\alpha}^\dagger$ are the coupling matrix elements between the electrodes and the scattering region. The Hamiltonians can be calculated through several approaches (e.g., using tight-binding methods). Actually, H_S is a functional of electronic density and for this reason, we used the Hamiltonian obtained from the DFT calculations. The charge density is self-consistently calculated via Green's functions until convergence is achieved; the transmission coefficient $T(E)$ can be obtained as:

$$T(E) = \Gamma_{\mathrm{L}}(E,V)\,\mathcal{G}(E,V)\,\Gamma_{\mathrm{R}}(E,V)\,\mathcal{G}^{\dagger}(E,V)$$

where the coupling matrices are given by $\Gamma_\alpha = i\left[\Sigma_\alpha - \Sigma_\alpha^\dagger\right]$, with $\alpha \equiv \{\mathrm{L},\mathrm{R}\}$. Further details regarding the methods for calculating electronic transport properties can be found in the literatures [51,58].

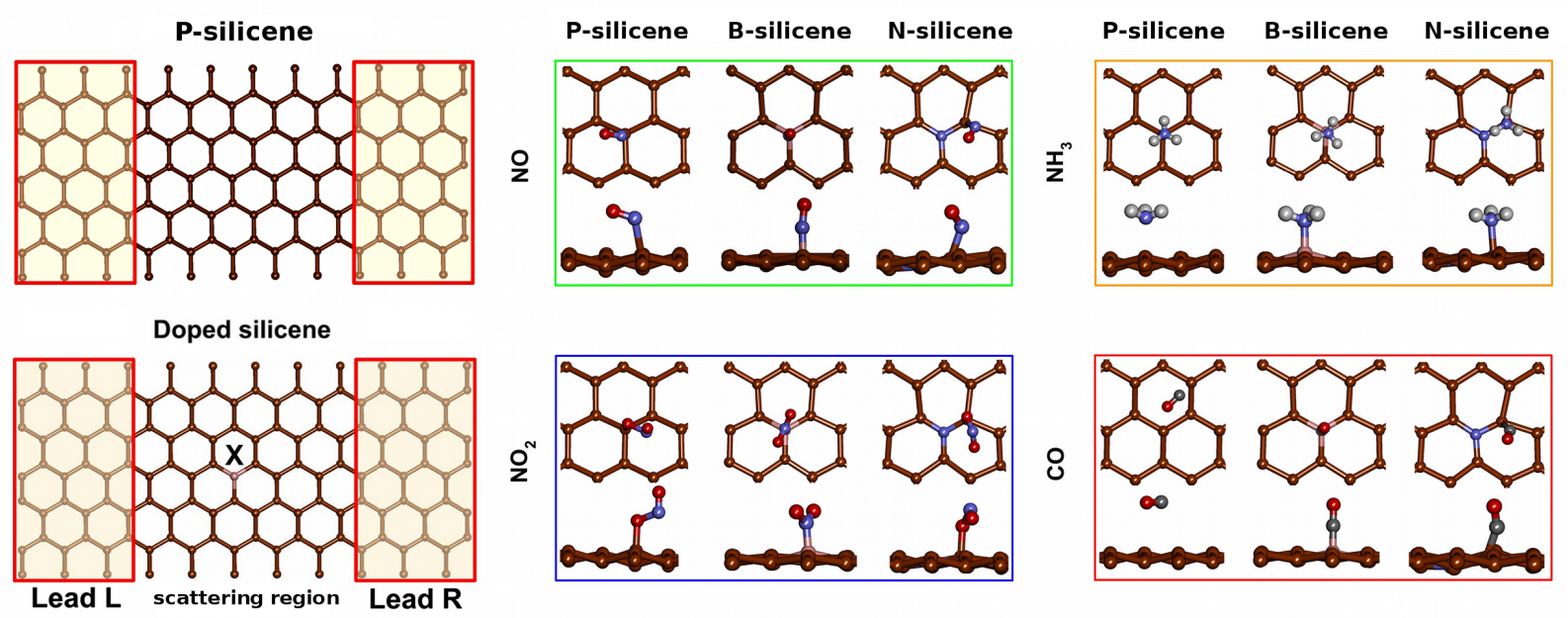

Figure 3.2: The device setup is shown in the left panel for pristine (upper) and doped silicene (lower) where X marks the site for B and N doping. The central and right panels show the most stable congurations for the four gas species NO, NH_3, NO_2 and CO when adsorbed on either pristine, B-doped or N-doped silicene.

Figure 3.2 shows a schematic device setup for P- and (B and N) doped-silicene used for gas detection. First, we address the structural stability of molecular adsorption geometries by initially placing each molecule on P- and B/N- silicene, respectively. Figure 3.3 shows four possible adsorption sites of gases on the P-silicene. They are referred to as the (I) hill, (II) valley, (III) bridge, and (IV) hollow sites. For doped sensors (B and N), only the gas adsorption above the B and N atoms and their nearest neighbors were tested. For these positions, different molecular orientations were examined. For diatomic gases (CO and NO), we investigated three possible orientations. Their molecular axis was oriented parallel and perpendicular (with the O pointing up and down) with respect to the silicene surface. For tri- and tetra- atomic gases (NO_2 and NH_3), two orientations were tested, i.e., one with the N atom pointing to the surface and the other with the N atom pointing away from the surface.

For P-silicene, twelve starting configurations for CO and NO (diatomic gases) and eight for NO_2 and NH_3 (tri-/tetra- atomic gases) were considered. Note that the starting configuration was not the final one. We sometimes see energy degenerated structures with very small binding energy differences. CO has two degenerate adsorption configurations, i.e., III-3 and IV-3. NO exhibits two most stable configurations, i.e., II-2 and III-2. NH_3 presents two degenerate adsorption configurations, i.e, IV-1 and II-1. The most stable configurations including its binding energy and binding distance are presented in Figure 3.2.

For P-silicene, in principle, there is no favorable site to adsorb the molecular gas. The interaction of NH_3 and CO with P-silicene is mostly of van der Waals type, whereas NO and NO_2 exhibit covalent chemisorption bonding. For doped devices, the gas molecules energetically prefer to be chemisorbed on the top of a B atom for B-silicene and chemisorbed on the top of a Si atom nearest to the N dopant for N-silicene. The binding energies of doped-silicene become larger than that of pristine, and the binding distances between the gases and doped-devices are shortened (see Table 3.1) as expected.

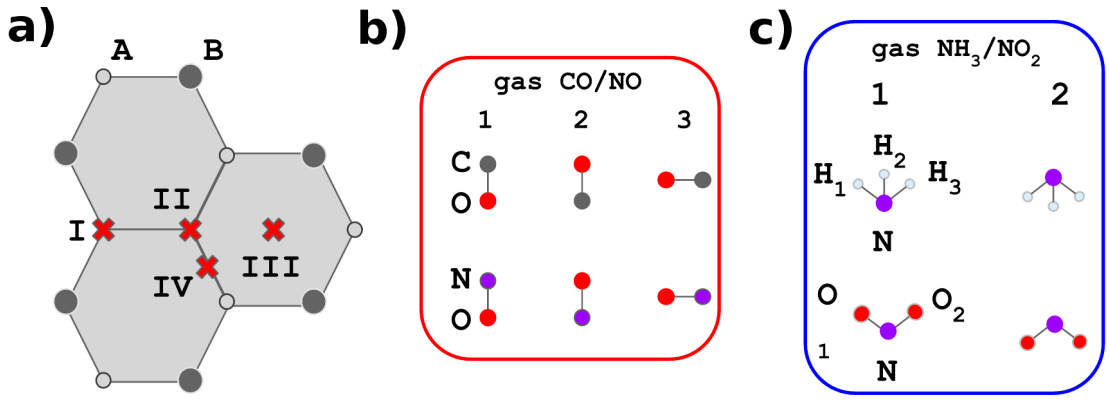

Figure 3.3: (a) Possible adsorption sites of gases on the hexagonal lattice of P-silicene: (I) hill, (II) valley, (III) bridge, and (IV) hollow sites. Different molecular orientations were examined for (b) CO and NO (diatomic gas molecules) with three possible orientations and (c) NH_3, and NO_2 (tri- and tetra-atomic gas molecules) with two initial orientations.

For doped-silicene, we examined only the gas adsorption above the dopants and their nearest neighbors since these adsorption sites are the most active. As shown in the main manuscript, we observed that different gases exhibit distinct configurations for each doped-silicene device. CO and NO (diatomic gases) binding with the doped-silicene at the C and N atom, respectively. They were tilted with respect to the surface for N- silicene, but aligned perpendicularly for B-silicene. NH_3 bonds to the silicene with its N atom for both doped-devices. NO_2 bonds to B-silicene with its N atom (B-N bond) and to N-silicene with an O atom (Si--O bond).

To better understand the binding strength of gas adsorption, we analyzed the charge density of three nanosensors, i.e. pristine and with the two dopants, as shown in Figure 3.4. The pristine device was considered a neutral device, in which the charge density is equally distributed through the device. Although the doped nanodevices were also neutral, they had charge localization in the vicinity of each dopant that led to the conclusion that atoms had electron donor and acceptor characteristics for B and N dopants, respectively. We furthermore considered the electronegativity of all species involved in the devices. For B-silicene, the charge is concentrated close to B (it became slightly negative) and the three nearest-neighbor Si partially share this charge. The second device doped with N has higher charge accumulation close to N, compared to the former case, and the neighbor Si atoms become less charged. These facts are due to the electronegativity hierarchy of Si and dopant atoms; (N < B < Si). N has a tendency to attract electrons more strongly than B and Si. Figure 3.4 confirms this assumption

that the charge was localized on the dopant for N-silicene and spread up the bonds for the B-silicene system.

Table 3.1: Calculated binding energy E_b , binding distance (D) and charge transfer from the silicene to molecules $\Delta Q(|e|)$

devices	gas	E_b (eV)	D (Å)	$\Delta Q(\|e\|)$
P-Silicene	NO	-0.73	2.11	0.19
	NO_2	-1.30	1.77	0.37
	NH_3	-0.26	2.27	0.16
	CO	-0.10	3.24	-0.03
B-Silicene	NO	-1.01	1.46	0.19
	NO_2	-3.02	1.50	0.08
	NH_3	-0.80	1.63	0.49
	CO	-1.19	1.51	0.32
N-Silicene	NO	-1.95	1.87	0.01
	NO_2	-3.50	1.76	-0.06
	NH_3	-0.80	2.06	0.42
	CO	-0.99	1.88	0.20

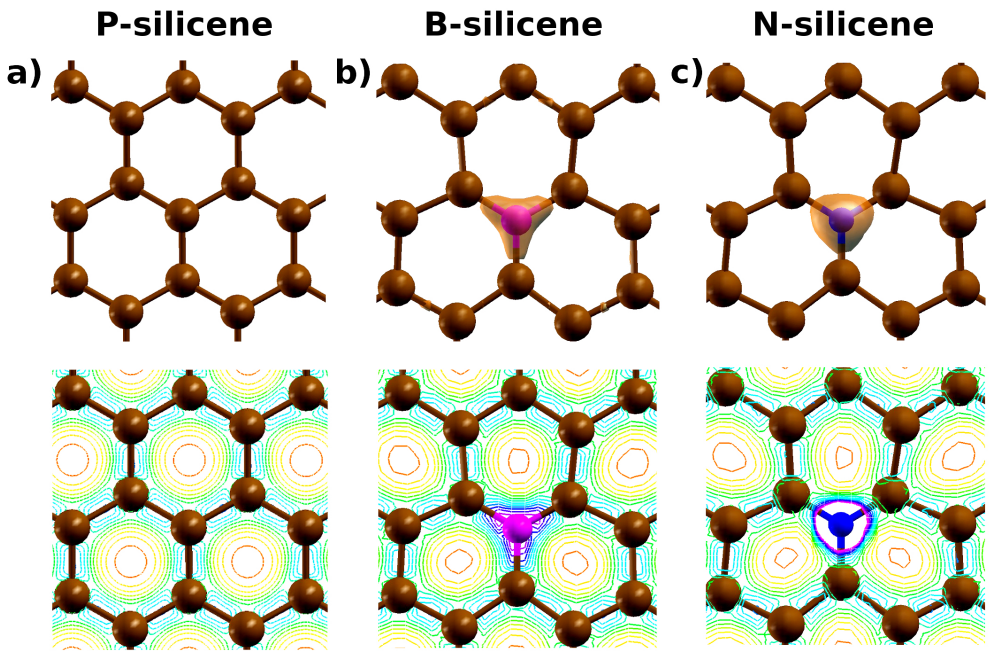

Figure 3.4: Charge density for (a) pristine silicene; (b) B-doped silicene and (c) N-doped silicene. The plotted isosurface corresponds to a value of 0.08$e \times bohr^{-3}$ for all panels.

The binding sites and molecular orientations of adsorbed gases on the nanosensor devices (Figure 3.2) needs to be discussed in more detail. For example, NO with an odd number of valence electrons has one unpaired electron on N atom which makes it highly reactive. As a result, NO always binds to the pristine silicene with N atom (see panel NO in center of Figure 3.2). As the second case in point, NH_3 has a tendency to bind to the pristine system with N, while the three H atoms point up. This is the simplest case because NH_3 has a lone pair on a N atom. The interesting case is for N-silicene, both dopant and gas have N atoms with the same electronegativity. Consequently, the NH_3 prefer binding with one Si atom close to a N atom (see Figure 3.2). Comparing the adsorption of NH_3, NO and NO_2 on P-silicene with previously reported results [37], our calculated binding energies are seen to differ in general by less than approximately 18%, however, the disagreement is larger for NH_3. When compared to the binding energy and the charge transfer of NH_3 on P-silicene in Ref. 61, our results agree quite well; there is a difference of 28.8% for binding energy and the value of charge transfer is exactly the same. The variation in results could be due to the difference of localized basis and plane-wave basis as well as the difference of dispersion correction. Additionally, our results are found to be in good agreement with

a previous DFT study \cite{Feng:2014ip} except for the cases of physisorbed gases, i.e., CO and NH_3. The binding energy difference between those results and ours for NH_3 amounts to almost 60%. This large discrepancy stems from the inclusion of the long-range van der Waals (vdW) interactions in our present work. Furthermore, we systematically optimized the adsorption geometry of each gas molecule considering various possible molecular orientations and adsorption sites as a starting point for each relaxation. Overall, we find qualitatively good agreement with previous studies for the most stable configuration of the adsorbate on P-silicene. However, when the device is doped, the gas prefers binding to the devices with a C atom. Finally, for NO_2 on P- and N-silicene devices, a covalent bond is formed between the Si atom and O atom due to the existence of an unpaired electron on one of the O atoms. For B-silicene, it is more energetically favorable that NO_2 binds to the system with its N atom. This results from the coordinate covalent bond in which an electron pair on the N atom enter to a vacant p-orbital on the B atom.

3.2 Possibility of Silicene Device as a Gas Sensor

Two of the most important challenges to build a good commercial sensor are the ability to detect different harmful gases (selectivity) and to improve the ability to sense some gas molecules (sensitivity). Experimentally, one of the most important parameters for sensing a gas is usually a variation in resistance or conductance, known as sensitivity. This property can be defined as $S(\%) = \frac{|G - G_0|}{G_0}$, where G and G_0 are the zero bias conductance for nanosensor with and without gas, respectively. Here, the conductance was simply calculated as $G = G_0 T(E_F)$, where $G = G_0 T(E_F)$ is the quantum conductance, e is the charge of the electron and h is Planck's constant.

The transmittance $T(E)$ of the P-, B- and N- silicene devices is presented in Figure 3.5-(a),(b),(c), respectively. Obviously, the gas adsorption significantly affects the $T(E)$of the three devices. For example, the adsorption of NO and NO_2 on P-silicene results in a remarkable decrease of the $T(E)$, whereas for CO and NH_3 the changes are not very pronounced. Additionally, the results indicate that doping either B or N atoms into silicene improves the detection of CO and NH_3, compared to that of P-silicene. Without the presence of gas, the $T(E)$ of doped-silicene was lower than that of the P-silicene (as depicted by the black dashed line in Figure 3.5. The $T(E)$ of B-silicene was lower than that of N-silicene. It was shown that the gas adsorption on the B-silicene device affected the $T(E)$, but not as strongly as for N-silicene.

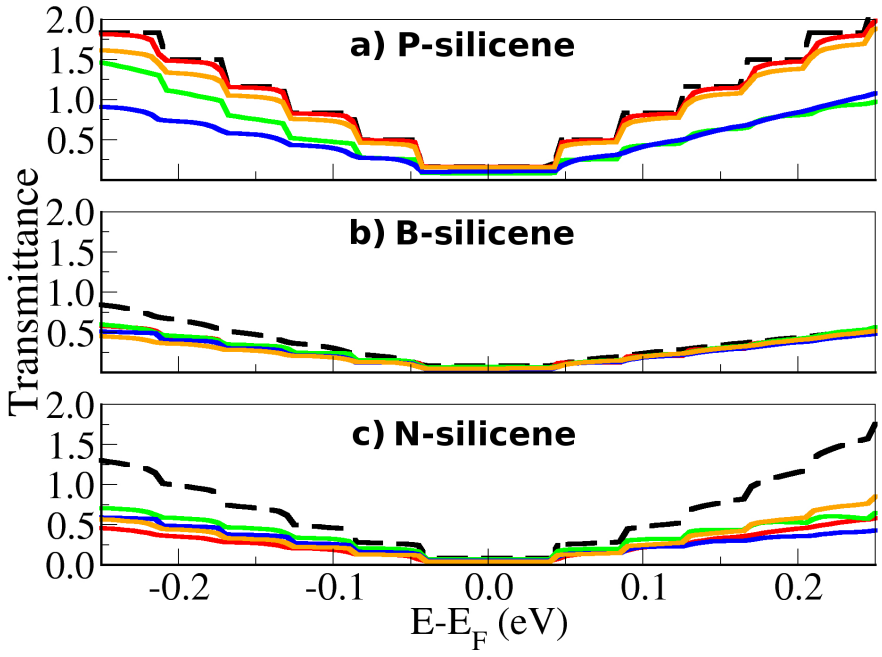

Figure 3.5: Transmittance as a function of energy, where the Fermi energy (E_F) is set at zero, is shown for (a) P-silicene; (b) B-silicene and (c) N-silicene. Red, green, orange and blue lines represent the transmittance for CO, NO, NH_3 and NO_2 adsorbed on the devices, respectively, while black dashed lines represent that of the reference system (P-,B- and N-silicene devices without gas).

Fig. 3.6-a presents the sensitivity as a function of binding energy of the three devices (P-, B-, and N- silicene) for NO, NO_2, NH_3 and CO gas molecules. In order to evaluate whether silicene and doped silicene can be good gas nanosensors, we should have both high and distinct sensitivities when the sensor is exposed to different gases. Another important aspect is about how long the gas can stay on the device. This is the translocation time τ and it is proportional to $\approx \exp\left(\frac{-E_b}{k_B T}\right)$,where E_b is binding energy, k_B is the Boltzmann constant and T is temperature. We expect small binding energies to lead to fast desorption of gases from the devices. Analyzing Figure 3.6-a, we found that the binding energies were generally less than 2 eV. The only exception occurred for NO_2 on the doped-devices ($E_b > 3$ eV). Turning our focus to each device, we observed that the P-silicene device (see Figure 3.6-b) has binding energies range from -0.1 to -1.3 eV and their respective sensitivities were strongly dependent on gas molecules. The sensitivity of the P-silicene device increased linearly with increasing binding energy. The sensitivities were found to follow an ascending order, i.e., CO < NH_3 < NO < NO_2. However, CO and NH_3 have low sensitivity. Spin-polarized calculations were also performed, but the resulting energy differences are smaller than the thermal

fluctuations at the envisioned operating temperature of the sensor, namely room temperature ($k_BT \approx 0.025$ eV). In a test, we found that the transmittance for each channel (up and down) exhibits only minor quantitative differences which do not affect our conclusions. For these reasons, spin polarization effects were neglected in our study.

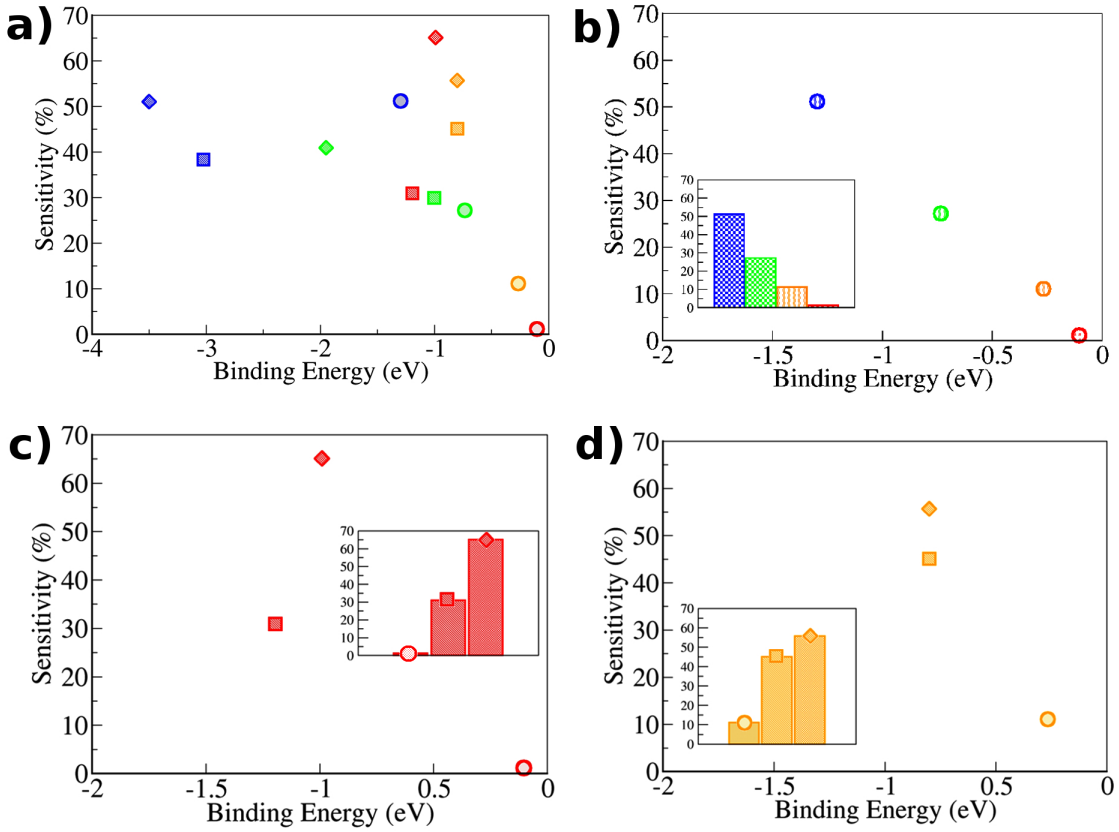

Figure 3.6 (a) Sensitivity versus binding energy for NO (green), NO_2 (blue), NH_3 (orange) and CO (red) gas molecules on P-silicene (circle), B-silicene (square) and N-silicene (diamond) devices, respectively; (b) the four gas species on P-siliene (the inset shows the sensitivity comparison for P-silicene); (c) CO on three devices and (d) NH_3 on three devices. The insets of (c) and (d) are the sensitivity comparison for one gas on the three different devices.

Next, we will address how to improve the sensitivity of these gases. As can be seen in Figure 3.5-a, by the introduction of dopant atoms, N-silicene (diamond shape) and B-silicene (square shape) exhibited higher binding energies and subsequently sensitivity.

This is especially true for CO and NH_3 (see Figure 3.6-c and 3.6-d). Better sensitivity was obtained due to increased binding energies (see Table 1). Interestingly, CO molecules can distinguish p-type and n-type doping of silicene (see Figure 3.5-c). This contradicts the findings of a previous study of a graphene-based gas sensor [60]. The CO on N-doped silicene showed a sensitivity around two orders of magnitude higher than that of CO on B-doped silicene. To explain why the sensitivity increased substantially for these molecular gases, the charge transfer of these systems will be investigated.

The transport properties of silicene devices relate to the change in local charge distribution around the B and N impurity atoms as a consequence of the charge transfer from gas molecules adsorbed on silicene. To visualize the charge transfer of NH_3 and CO adsorbed on the devices, we calculate the charge density difference: $\Delta\rho(\vec{r}) = \rho_{device+gas}(\vec{r}) - (\rho_{device}(\vec{r}) + \rho_{gas}(\vec{r}))$, as presented in Figure 3.7. The contour plot of $\Delta\rho$ illustrates the charge accumulation/depletion in the system, i.e., we can quantitatively describe the idea of the charge transfer. For doped silicene, there is charge accumulation indicating the hybridization of orbitals at the nanosensor surface in which NH_3 and CO is adsorbed (see Figure 3.7). Such orbital hybridization is absent for physisorption of the gases on P-silicene. In other words, the charge-transfer capability increases with the increasing bonding charge densities.

Furthermore, we investigated the electron charge transfer using the Mulliken population analysis (see Table 1). It is notable that the positive charge transfer occurred from the gas molecules to the silicene. As discussed above, our results reveal the difference in charge redistribution of three nanosensors (see Figure 3.7). For B-silicene, as shown in Table 1 all gases examined in the current study act as donors. They donate charges to the device, resulting from the vacant p-orbital on the B atom. A large amount of charge transfer is obtained, especially for NH_3, which is electron-donating molecule. For N-silicene, the electron-rich gas molecules prefer to adsorb on the top of one positively charged Si close to N (see Figure 3.2). A negative charge transfer value as observed only for NO_2 due to its strong electron-withdrawing capabilities.

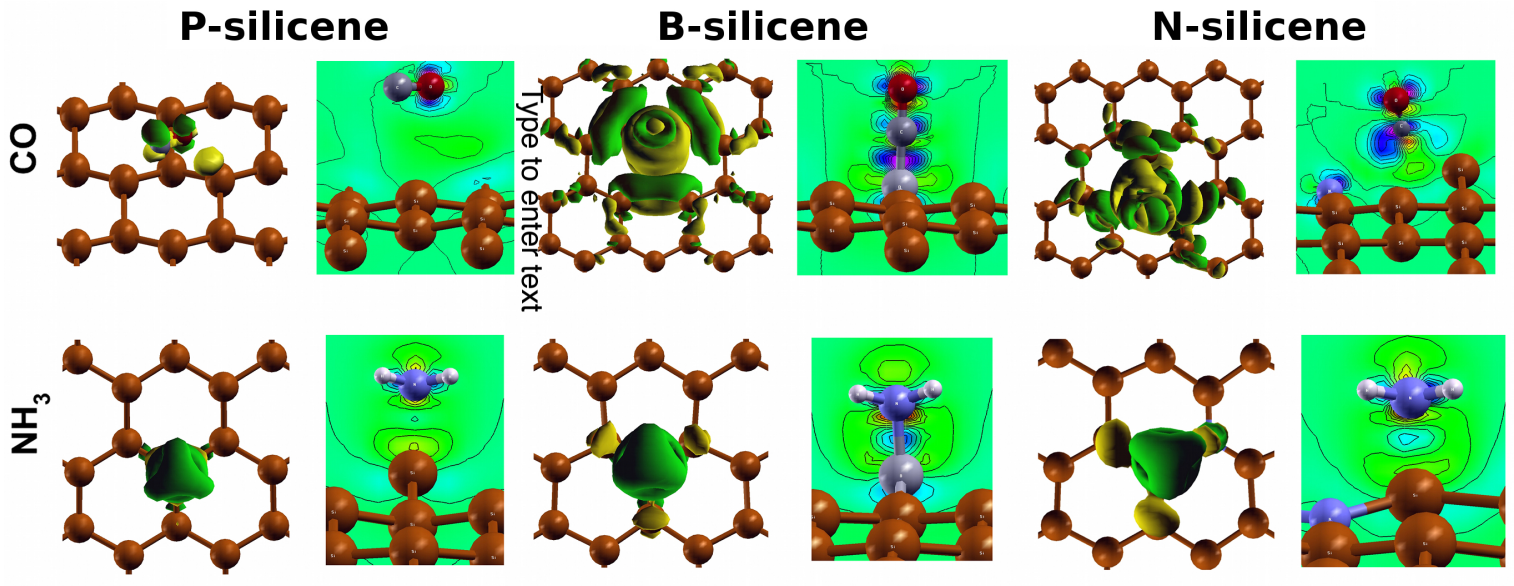

Figure 3.7: Charge density difference for CO (upper) and NH_3 (lower panel) on P-, B-, and N-silicene devices for each type of nanosensor. Isosurfaces are plotted for isovalues of 0.0004 (0.002) $e \times bohr^{-3}$ for CO (NH_3) alongside contour plots. For the isosurface plots, green color represents negative charge density difference while yellow corresponds to a positive change in charge density.

A few important aspects should also be discussed. The first is the influence of substrates on gas sensing performance. According to the experimental studies, for all the cases, silicene was synthesized on top of some substrates [14,22,23,25]. A very recent study [36] elaborated the effect of Ag(111) substrate on the electronic structures of gas molecules on silicene, indicating a slight increase in adsorption energies and charge transfer. We expected that the conductance could be changed due to the influence of different substrates, changing the sensitivity, but the interaction between silicene should not substantially change the overall trend with this additional component. The second point is about the experimental challenge to control the doping in silicene. Recent experimental studies reported on potassium adsorption in silicene [62], inducing n-type doping. Additionally, a theoretical study also showed the stability of B/N substituted doping into silicene [63]. Therefore, if reactive centers can be created as we have shown, their gas sensing performance will be improved enormously. In addition, there remain many challenging problems. For instance, a recent study [64] demonstrated the dissociative adsorption of molecules (H_2, O_2, CO, H_2O and OH) on defect sites in graphene and silicene. In our study, these molecules remain intact on silicene, but certain molecules may dissociate due to increased chemical reactivity at the defect sites as it has been reported previously [62].

CHAPTER IV
Conclusions

In conclusion, we investigated the capability of silicene-based devices for sensing chemical gases in terms of sensitivity and selectivity. We employed rst-principles electronic structure calculations based on density functional theory formalism. For adsorption of NO, NO_2, NH_3 and CO on pristine (P-), B-doped or N-doped silicene, we determine the adsorption congurations, binding energies, charge transfer and change in the electronic transport properties. Our results reveal that P-silicene can detect NO and NO2 gas molecules with high sensitivity. However, this is limited to CO and NH_3 due to weak van derWaals interaction between those gases and P-silicene. By doping P-silicene with either B or N atoms, enhanced binding and charge transfer of all studied gases on the nanosensor were achieved, resulting in an increased sensitivity towards NH3 and CO detection. However, doped-silicene strongly bound to NO and NO_2 is not presumably suitable for practical gas sensor devices. Based on our results, we can conclude that by doping with different impurities, one can create a silicene device that is able to detect different gas species with high sensitively and selectivity.

Acknowledgements

I would like to thank Associated Professor Vittaya Amornkitbamrung who is my mentor for his constructive and useful suggestions. I would also like to thank the Integrated Nanotechnology Research Center (INRC), Nanotec-KKU Center of Excellence on Advanced Nanomaterials for Energy Production and Storage, Thailand. Last but not least, this project is financially supported by The Thailand Research Fund (TRF), the Commission on Higher Education (CHE), and Nakhon Phanom University under contract number MRG5680186.

References

[1] Watson, J; and Ihokura, K. Gas-sensing materials MRS Bull., **1999**, 14, 24.

[2] Dong Lee, D. D and Lee, D. S. Environmental gas sensors Sensors Journal, IEEE. **2001**,, 1(3), 214.

[3] Schedin, F.; Geim, A. K.; Morozov, S. V.; Hill, E. W.; Blake, P.; Katsnelson, M. I.; Novoselov, K. S. Detection of Individual Gas Molecules Adsorbed on Graphene. Nat. Mater. **2007**, 6, 652-655.

[4] He, Q.; Wu, S.; Yin, Z.; Zhang, H. Graphene -Based Electronic Sensors. Chem. Sci. **2012**,3, 1764-1772.

[5] Fowler, J. D.; Allen, M. J.; Tung, V. C.; Yang, Y.; Kaner, R. B.; Weiller, B. H. Practical Chemical Sensors from Chemically Derived Graphene. ACS Nano **2009**, 3, 301-306.

[6]. Some, S.; Xu, Y.; Kim, Y.; Yoon, Y.; Qin, H.; Kulkarni, A.; Kim, T.; Lee, H. Highly-Sensitive and Selective Gas Sensor Using Hydrophilic and Hydrophobic Graphenes. Sci. Rep. **2013**, 3, 1868.

[7] Deng, S.; Tjoa, V.; Fan, H. M.; Tan, H. R.; Sayle, D. C.; Olivo, M.; Mhaisalkar, S.; Wei, J.; Sow, C. H. Reduced Graphene Oxide Conjugated Cu2O Nanowire Mesocrystals for High-Performance NO2 Gas Sensor. J. Am. Chem. Soc. **2012**, 134, 4905.

[8] Leenaerts, O.; Partoens, B.; Peeters, F. Adsorption of H2O, NH3, CO, NO2, and NO on Graphene: A First-Principles Study. Phys. Rev. B **2008**, 77, 125416.

[9]. Zhang, Y.-H.; Chen, Y.-B.; Zhou, K.-G.; Liu, C.-H.; Zeng, J.; Zhang, H.-L.; Peng, Y.Improving Gas Sensing Properties of Graphene by Introducing Dopants and Defects: A First-Principles Study. Nanotechnology **2009**, 20, 185504.

[10] Dai, J.; Yuan, J.; Giannozzi, P. Gas Adsorption on Graphene Doped with B, N, Al, and S: A Theoretical Study. Appl. Phys. Lett. **2009**, 95, 232105.

[11] Cahangirov, S.; Topsakal, M.; Akturk, E.; Sahin, H.; Ciraci, S. Two- and One-Dimensional Honeycomb Structures of Silicon and Germanium. Phys. Rev. Lett. **2009**, 102, 236804.

[12] Jose, D.; Datta, A. Structures and Chemical Properties of Silicene: Unlike Graphene. Acc. Chem. Res. **2014**, 47, 593-602.

[13] Lin, X.; Ni, J. Much Stronger Binding of Metal Adatoms to Silicene than to Graphene:A First-Principles Study. Phys. Rev. B **2012**, 86, 075440.

[14] Vogt, P.; De Padova, P.; Quaresima, C.; Avila, J.; Frantzeskakis, E.; Asensio, M. C.; Resta, A.; Ealet, B.; Le Lay, G. Silicene: Compelling Experimental Evidence for Graphenelike Two-Dimensional Silicon. Phys. Rev. Lett. **2012**, 108, 155501.

[15] Houssa, M.; van den Broek, B.; Scalise, E.; Pourtois, G.; Afanas'ev, V. V.; Stesmans, A. An electric eld tunable energy band gap at silicene/(0001) ZnS interfaces. Phys. Chem. Chem. Phys. **2013**, 15, 3702{3705.

[16] Drummond, N. D.; Zolyomi, V.; Fal'ko, V. I. Electrically Tunable Band Gap in Silicene Phys. Rev. B **2012**, 85, 075423.

[17] Kaloni, T. P.; Schreckenbach, G.; Freund, M. S. Large Enhancement and Tunable Band Gap in Silicene by Small Organic Molecule Adsorption. J. Phys. Chem. C **2014**, 118, 23361-23367.

[18] Denis, P. A. Stacked Functionalized Silicene: A Powerful System to Adjust the Electronic Structure of Silicene. Phys. Chem. Chem. Phys. **2015**, 17, 5393-5402.

[19] Kaloni, T. P.; Singh, N.; Schwingenschlogl, U. Prediction of a Quantum Anomalous Hall State in Co-Decorated Silicene Phys. Rev. B **2014**, 89, 035409.

[20] Houssa, M.; Pourtois, G.; Heyns, M. M.; Afanas'ev, V. V.; Stesmans, A. Electronic Properties of Silicene: Insights from First-Principles Modelling. ECS Trans. **2010**, 33, 185-193.

[21] Lazar, P.; Karlick, F.; Jureka, P.; Kocman, M.; Otyepkov, E.; afov, K.; Otyepka, M. J. Am. Chem. Soc. **2013**, 135, 6372-6377.

[22] Feng, B.; Ding, Z.; Meng, S.; Yao, Y.; He, X.; Cheng, P.; Chen, L.; Wu, K. Evidence of Silicene in Honeycomb Structures of Silicon on Ag(111). Nano Lett. **2012**, 12, 3507-3511.

[23] Rachid Tchalala, M.; Enriquez, H.; Mayne, A. J.; Kara, A.; Roth, S.; Silly, M. G.; Bendounan, A.; Sirotti, F.; Greber, T.; Aufray, B. et al. Formation of One-Dimensional Self-Assembled Silicon Nanoribbons on Au(110)-(21). Appl. Phys. Lett. **2013**, 102, 083107.

[24] Fleurence, A.; Friedlein, R.; Ozaki, T.; Kawai, H.; Wang, Y.; Yamada-Takamura, Y. Experimental Evidence for Epitaxial Silicene on Diboride Thin Films. Phys. Rev. Lett. **2012**, 108, 245501.

[25] Meng, L.; Wang, Y.; Zhang, L.; Du, S.; Wu, R.; Li, L.; Zhang, Y.; Li, G.; Zhou, H.; Hofer, W. A. et al. Buckled Silicene Formation on Ir(111). Nano. Lett. **2013**, 13, 685–690.

[26] Tsai, W.-F.; Huang, C.-Y.; Chang, T.-R.; Lin, H.; Jeng, H.-T.; Bansil, A. Gated silicene as a tunable source of nearly 100 % spin-polarized electrons. Nat. Comm. **2013**, 4, 1500.

[27] Xu, C.; Luo, G.; Liu, Q.; Zheng, J.; Zhang, Z.; Nagase, S.; Gao, Z.; Lu, J. Giant Magnetoresistance in Silicene Nanoribbons . Nanoscale **2012**, 4, 3111–3117.

[28] Ni, Z.; Zhong, H.; Jiang, X.; Quhe, R.; Luo, G.; Wang, Y.; Ye, M.; Yang, J.; Shi, J.; Lu, J. Tunable Band Gap and Doping Type in Silicene by Surface Adsorption: Towards Tunneling Transistors. Nanoscale **2014**, 6, 7609–7618.

[29] Liu, H.; Gao, J.; Zhao, J. Silicene on Substrates: A Way to Preserve or Tune Its Electronic Properties. J. Phys. Chem. C **2013**, 117, 10353–10359.

[30] Ni, Z.; Liu, Q.; Tang, K.; Zheng, J.; Zhou, J.; Qin, R.; Gao, Z.; Yu, D.; Lu, J. Tunable Bandgap in Silicene and Germanene. Nano Lett. **2011**, 12, 113–118.

[31] Tao, L.; Cinquanta, E.; Chiappe, D.; Grazianetti, C.; Fanciulli, M.; Dubey, M.; Molle, A.; Akinwande, D. Silicene Field-Effect Transistors Operating at Room Temperature. Nat. Nanotech. **2015**, 10, 227–231.

[32] Jose, D.; Datta, A. Structures and Electronic Properties of Silicene Clusters: A Promising Material for FET and Hydrogen Storage. Phys. Chem. Chem. Phys. **2011**, 13, 7304–7311.

[33] Hussain, T.; Chakraborty, S.; Ahuja, R. Metal-Functionalized Silicene for Efficient Hydrogen Storage. Phys. Chem. Chem. Phys. **2013**, 14, 3463–3466.

[34] Sadeghi, H.; Bailey, S.; Lambert, C. J. Silicene-Based DNA Nucleobase Sensing. Appl. Phys. Lett. **2014**, 104, 103104.

[35] Amorim, R. G.; Scheicher, R. H. Silicene as a New Potential DNA Sequencing Device. Nanotechnology **2015**, 26, 154002.

[36] Feng, J.-w.; Liu, Y.-j.; Wang, H.-x.; Zhao, J.-x.; Cai, Q.-h.; Wang, X.-z. Gas Adsorption on Silicene: A Theoretical Study. Comp. Mater. Sci. **2014**, 87, 218–226.

[37] Hu, W.; Xia, N.; Wu, X.; Li, Z.; Yang, J. Silicene as a Highly Sensitive Molecule Sensor for NH_3, NO and NO_2. Phys. Chem. Chem. Phys. **2014**, 16, 6957–6962.

[38] Richard M. Martin. Electronic Structure: Basic Theory and Practical Methods. Cambridge University Press, **2004**.

[39] Sholl, D. S. and Steckel, J. A. Density Functional Theory: A Practical Introduction. A JOHN WILEY & SONS, INC., **2009**.

[40] Jensen, F. Introduction to Computational Chemistry. John Wiley & Sons, Ltd., 2007.

[41] Kohn, W; Becke, A. D. and Parr, R. G. Density functional theory of electronic structure. J. Phys. Chem, 100:12974–12980, **1996**.

[42] Robert G. Parr. Density functional theory. Ann. Rev. Phys .Chem., 34:631–656, 1983.

[43] Hohenberg, P. and Kohn, W. Phys. Rev., **1964**, 136:B864.

[44] Kohn, W and Sham, L. J. Phys. Rev., **1965**, 136:A1133.

[45] Perdew, J. P. and Wang, Y. Accurate and simple analytic representation of the electron-gas correlation energy. Phys. Rev. B, **1992**, 45:13244–13249.

[46] Perdew, J. P.; Burke, K. and Ernzerhof, M. Generalized gradient approximation made simple. Phys. Rev. Lett, **1996**, 77:3865.

[47] Perdew, J. P; Ruzsinszky, A; Tao, J.; Staroverov, V. N.; Scuseria, G. E.; and Csonka, G. I. J. Chem. Phys., **2005**, 123:62201.

[48] Crljen, Z.; Sokcevic; D; Brako, R. and P. Lazic. Phys. Rev. B., **2003**, 68:195411.

[49] Soler, J. M.; Ordejon, P.; Artacho, E. Self-consistent order-n density-functional calculations for very large systems. Phys. Rev. B, **1996**, 53:R10441.

[50] Rocha, A. R.; Garcia-Suarez, V. M. and S Bailey. Towards molecular spintronics. Nat. Mater., **2005**, 4:335–339.

[51] Rocha, A. R.; Garcia-Suarez, V. M.; Bailey, S.; Lambert, C; Ferrer, J. and Sanvito, S. Spin and molecular electronics in atomically generated orbital landscapes. Phys. Rev. B, **2006**, 73:085414.

[52] Kittel, C. Introduction to Solid State Physics: 8th edition. JohnWiley & Sons, Ltd., **2005**.

[53] Troullier, N. and Martins, J. L. Efficient pseudopotentials for plane-wave calculations. Phys. Rev. B. **1991**,43, 1993-2006.

[54] Kerker, G. P. J. Phys. C: Solid State Phys. **1980**, 13, L189–L194.

[55] DiVentra, M. Electrical Transport in Nanoscale Systems. Cambridge University Press, **2008**.

[56] Dion, M.; Rydberg, H.; Schroder, E.; Langreth, D. C.; Lundqvist, B. I. Van der Waals Density Functional for General Geometries. Phys. Rev. Lett. **2004**, 92, 246401.

[57] Roman-Perez, G.; Soler, J. Ecient Implementation of a van der Waals Density Functional: Application to Double-Wall Carbon Nanotubes. Phys. Rev. Lett. **2009**, 103, 096102.

[58] Brandbyge, M.; Mozos, J.-L.; Ordejon, P.; Taylor, J.; Stokbro, K. Density-Functional Method for Nonequilibrium Electron Transport. Phys. Rev. B **2002**, 65, 165401.

[59] 36. Hu, W.; Xia, N.; Wu, X.; Li, Z.; Yang, J. Silicene as a Highly Sensitive Molecule Sensor for NH_3, NO and NO_2. Phys. Chem. Chem. Phys. **2014**, 16, 6957-6962.

[60] Zhang, Y.-H.; Chen, Y.-B.; Zhou, K.-G.; Liu, C.-H.; Zeng, J.; Zhang, H.-L.; Peng, Y. Improving Gas Sensing Properties of Graphene by Introducing Dopants and Defects: A First-Principles Study. Nanotechnology **2009**, 20, 185504.

[61] Kaloni, T. P.; Schreckenbach, G.; Freund, M. S. Large Enhancement and Tunable Band Gap in Silicene by Small Organic Molecule Adsorption. J. Phys. Chem. C **2014**, 118, 23361-23367.

[62] Friedlein, R.; Fleurence, A.; Sadowski, J. T.; Yamada-Takamura, Y. Tuning of Silicene-Substrate Interactions with Potassium Adsorption. Appl. Phys. Lett. **2013**, 102, 221603.

[63] Sivek, J.; Sahin, H.; Partoens, B.; Peeters, F. M. Adsorption and Absorption of Boron, Nitrogen, Aluminum, and Phosphorus on Silicene: Stability and Electronic and Phonon Properties. Phys. Rev. B **2013**, 87, 085444.

[64] Grel, H. H.; zelik, V. O.; Ciraci, S. Dissociative Adsorption of Molecules on Graphene and Silicene. J. Phys. Chem. C **2014**, 118, 27574-27582.

Output

Outputs of this project are based on the following paper:

Prasongkit, J*.; Amorim, R. G.; Chakraborty, S.; Ahuja, R; Scheicher, R. H.; Amornkitbamrung, V. Highly Sensitive and Selective Gas Detection Based on Sillicene. *J. Phys. Chem. C*., **DOI:** 10.1021/acs.jpcc.5b03635

Note that * indicates the corresponding author.

Appendix

THE JOURNAL OF PHYSICAL CHEMISTRY C

Article

pubs.acs.org/JPCC

Highly Sensitive and Selective Gas Detection Based on Silicene

Jariyanee Prasongkit,*[,†,‡] Rodrigo G. Amorim,[¶,⊥] Sudip Chakraborty,[¶] Rajeev Ahuja,[¶,§] Ralph H. Scheicher,[¶] and Vittaya Amornkitbamrung[∥,‡]

[†]Division of Physics, Faculty of Science, Nakhon Phanom University, Nakhon Phanom, 48000, Thailand

[‡]Nanotec-KKU Center of Excellence on Advanced Nanomaterials for Energy Production and Storage, Khon Kaen, 40002, Thailand

[¶]Division of Materials Theory, Department of Physics and Astronomy, Uppsala University, Box 516, SE-751 20 Uppsala, Sweden

[§]Applied Materials Physics, Department of Materials Science and Engineering, Royal Institute of Technology (KTH), SE-100 44 Stockholm, Sweden

[∥]Integrated Nanotechnology Research Center, Department of Physics, Faculty of Science, Khon Kaen University, Khon Kaen, 40002, Thailand

Supporting Information

ABSTRACT: Recent advances in the fabrication of silicene devices have raised exciting prospects for practical applications such as gas sensing. We investigated the gas detection performance of silicene nanosensors for four different gases (NO, NO_2, NH_3, and CO) in terms of sensitivity and selectivity, employing density functional theory and nonequilibrium Green's function method. The structural configurations, adsorption sites, binding energies and charge transfer of all studied gas molecules on silicene nanosensors are systematically discussed in this work. Our results indicate that pristine silicene exhibits strong sensitivity for NO and NO_2, while it appears incapable of sensing CO and NH_3. In an attempt to overcome sensitivity limitations due to weak van der Waals interaction of those latter gas molecules on the device, we doped pristine silicene with either B or N atoms, leading to enhanced binding energy as well as charge transfer, and subsequently a significant improvement of sensitivity. A distinction between the four studied gases based on the silicene devices appears possible, and thus these promise to be next-generation nanosensors for highly sensitive and selective gas detection.

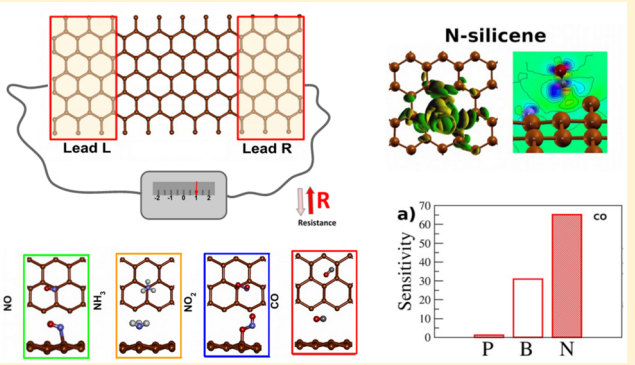

INTRODUCTION

Two-dimensional nanostructure materials have taken the front row in innovative applications in the past decade after the successful experimental exfoliation of graphene. Gas sensors based on graphene have attracted much attention since graphene has excellent sensitivity to detect various gas molecules, large sensing area per unit volume, low electronic temperature noise, fast response time, and high chemical stability.[1,2] The potential use of graphene for gas detection has been intensively investigated both experimentally[3−5] and theoretically.[6−8] However, growth of graphene over large surface areas is constrained. This motivated the search for other materials with similar favorable properties. In turn, this has led to the discovery of silicene as a silicon counterpart. The good properties with versatile silicon based nanotechnology gives the edge to silicene rather than graphene. This serves as the motivation of our work to theoretically explore the applicability of silicene for gas sensing.

The massless Dirac Fermions are the main reasons behind the ultrahigh carrier mobility for both the honeycomb structures of silicene and graphene.[9,10] Geometrically, the hexagonal structure of silicene has a larger size due to the larger ionic radius of Si atoms,[11] but they have similar electronic structures. One important demarcation between the two structures is a buckled formation in silicene. This is due to sp^3 and sp^2 hybridization[12] rather than only sp^2 hybridization. This feature leads to a few prominent differences in the properties of silicene and graphene. Band gap tuning with an external electric field[13,14] and with the binding adsorbates[15−17] can be seen more profoundly in silicene than in graphene.[18,19] Although free-standing silicene has not been achieved so far, recent progress shows that it can be synthesized experimentally by depositing silicon on different surfaces such as silver,[20,21] gold,[22] zirconium diboride,[23] and iridium.[24]

To date, a wide range of potential applications of silicene have been proposed in various field such as spintronics,[25,26] FETs,[27−30] hydrogen storage,[31,32] and sensing devices.[33,34] Nevertheless, using silicene as gas sensor has not been given the

Received: April 16, 2015
Revised: June 25, 2015

DOI: 10.1021/acs.jpcc.5b03635
J. Phys. Chem. C XXXX, XXX, XXX−XXX

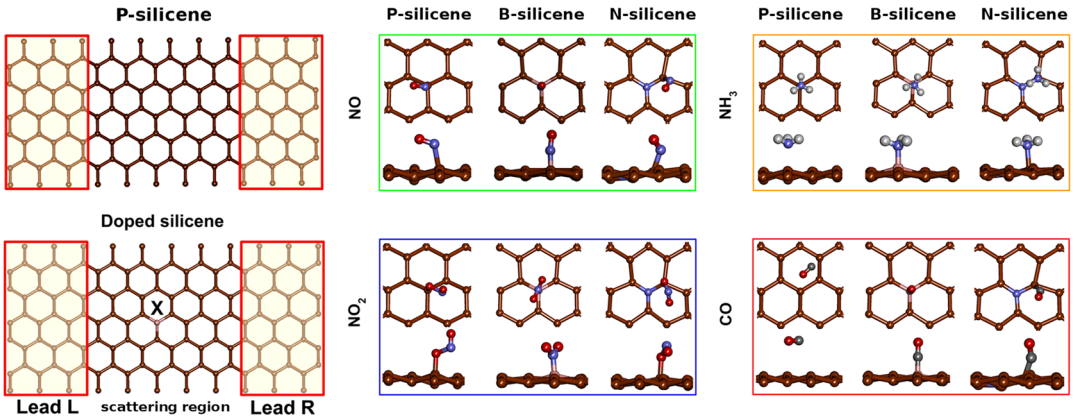

Figure 1. Device setup is shown in the left panel for pristine (upper) and doped silicene (lower) where X marks the site for B and N doping. The central and right panels show the most stable configurations for the four gas species NO, NH_3, NO_2, and CO when adsorbed on either pristine, B-doped or N-doped silicene.

attention it deserves. Two theoretical investigations based on density functional theory (DFT) were done to explore potential application of silicene as a molecular sensor for gas molecules.[35,36] They revealed changes in the electronic structures of silicene with adsorbed gas. The prime parameters to characterize the sensor performance of a gas sensor are sensitivity, selectivity, response time and recovery time. They should be addressed simultaneously to meet real application requirements of silicene based sensing systems.

The purpose of our study was therefore 2-fold. First, we used the state-of-the-art first-principle methods to study the electronic and transport properties to evaluate the gas discrimination of silicene in terms of sensitivity and selectivity. Second, we demonstrate the possibility to improve gas sensing performance of silicene through doping this material with B and N atoms.

In this work, we investigated the electronic and transport properties of gas molecules adsorbed onto pristine (P) and B/N-doped silicene by employing a robust combination of nonequilibrium Green's function (NEGF) techniques and DFT. Four representative gas species—NO_2, NO, NH_3, and CO molecules, which are of main interest for environmental safety and medical purposes, were shown to be detectable by silicene based sensor devices. The sensitivity and selectivity of the devices to the presence of those gas molecules were evaluated from the changes in their electronic transport properties. Our results indicate that doping impurity atoms into silicene can enhance the interaction between the gas molecules and doped devices. This enabled an immense improvement in the performance of this type of sensor.

■ COMPUTATIONAL METHODS

The geometrical structures of four different molecular gases (NO, NO_2, NH_3, and CO) adsorbed on pristine silicene and doped-silicene nanodevices were relaxed by using DFT[37,38] as implemented in the SIESTA package.[39] To describe the weak dispersive interactions, we employed a van der Waals correction[40,41] to the generalized gradient approximation of Perdew, Burke, and Ernzerhof (PBE-GGA)[42] for the exchange-correlation functional in DFT.

A description of van der Waals (vdW) were performed using vdW-DF, as proposed by Dion et al.[40] In this methodology, the exchange-correlation energy is written as

$$E_{xc} = E_x^{GGA} + E_c^{LDA} + E_c^{nl} \quad (1)$$

where the exchange energy E_x^{GGA} uses the GGA functional, and E_c^{LDA} is the local density approximation (LDA) to correlation energy. The nonlocal correlation-energy part, E_c^{nl}, is defined to include the longest-ranged or most nonlocal energy term which is zero for systems with constant density.

For the ionic relaxation 6 × 1 × 4 *k*-points and for the electronic transport 24 × 1 × 1 *k*-points were used. Furthermore, double-ζ polarized basis sets (DZP) and norm-conserving pseudopotentials[43] were used. The conjugate gradient (CG) method was applied to obtain equilibrium structures with residual forces on atoms below 0.01 eV/Å. We also employed VASP[44] code, using the same parameters as in of SIESTA for the relaxation and binding energy calculations with a 400 eV cutoff energy for the plane wave basis and a force tolerance of 0.01 eV/Å. Silicene has a buckled hexagonal lattice, consisting of 2 Si atoms per unit cell. For transport calculation, each simulated system consisted of 20.57 Å × 15 Å × 43.54 Å silicene supercell with 132 Si atoms. We use the periodic boundary condition (PBC) along the *x*-direction and the *z*-direction and considerably large supercell to avoid the interaction occurring between mirror images. The neighboring silicene in the *y*-direction was separated by 15 Å of vacuum. See Supporting Information for additional details on supercell construction.

The transport properties were then investigated with the TranSiesta code,[45] combining the NEGF method and DFT. This was done to perform electronic transport calculations in order to visualize the degree of capability of pristine silicene and doped-silicene nanodevices as an electric nanosensors to distinguish four different molecular gases (NO, NO_2, NH_3, and CO). The basis sets and the real-space grid employed in the transport calculations are identical to those described above for the geometrical optimization part. The system was divided into three parts: two leads (left and right) and a scattering region in between them. The left panel of Figure 1 shows upper (pristine) and lower panel (doped) hexagonal 2D silicene that was used as a molecular gas sensor. The red shaded rectangles represent the electrodes or leads (left/right) and the region in between was the scattering region. Nitrogen (N) and boron (B) are the two substituted atoms used to functionalize silicene.

Defining the boundary as a region, where the charge density matches with the bulk electrodes and using localized basis sets,

DOI: 10.1021/acs.jpcc.5b03635
J. Phys. Chem. C XXXX, XXX, XXX−XXX

the NEGF for the scattering region $\mathcal{G}(E, V)$ can be formulated as following:

$$\mathcal{G}(E, V) = [E \times S_S - H_S[\rho] - \Sigma_L(E, V) - \Sigma_R(E, V)]^{-1} \quad (2)$$

where S_S and H_S are the overlap matrix and the Hamiltonian, respectively, for the scattering region. $\Sigma_{L/R}$ are self-energies that account for the effect from the left (L) and right (R) electrodes upon the central region. The self-energies are given by $\Sigma_\alpha = V_{S\alpha} g_\alpha V_{\alpha S}$, where g_α are the surface Green's functions for the semi-infinite leads and $V_{\alpha S} = V_{S\alpha}^\dagger$ are the coupling matrix elements between the electrodes and the scattering region. The Hamiltonians can be calculated through several approaches (e.g., using tight-binding methods). Actually, H_S is a functional of electronic density and for this reason, we used the Hamiltonian obtained from the DFT calculations. The charge density is self-consistently calculated via Green's functions until convergence is achieved; the transmission coefficient $T(E)$ can be obtained as

$$T(E) = \Gamma_L(E, V)\mathcal{G}(E, V)\Gamma_R(E, V)\mathcal{G}^\dagger(E, V) \quad (3)$$

where the coupling matrices are given by $\Gamma_\alpha = i[\Sigma_\alpha - \Sigma_\alpha^\dagger]$, with $\alpha \equiv \{L, R\}$. Further details regarding the methods for calculating electronic transport properties can be found in the literature.[45,46]

RESULTS AND DISCUSSION

Adsorption Configurations. Figure 1 (left panel) shows a schematic device setup for P- and (B and N) doped-silicene used for gas detection. First, we address the structural stability of molecular adsorption geometries by initially placing each molecule on P- and B/N- silicene, respectively. For P-silicene, there are at least four possible starting adsorption sites: hill, valley, hollow and bridge sites. For doped sensors (B and N), only the gas adsorption above the B and N atoms and their nearest neighbors were tested. For these positions, different molecular orientations were examined. For diatomic gases (CO and NO), we investigated three possible orientations. Their molecular axis was oriented parallel and perpendicular (with the O pointing up and down) with respect to the silicene surface. For tri- and tetratomic gases (NO_2 and NH_3), two orientations were tested, i.e., one with the N atom pointing to the surface and the other with the N atom pointing away from the surface. The most stable adsorption configurations of each molecular gas on the silicene devices are presented in Figure 1 (central and right panels). A more detailed discussion of other less stable adsorption configurations can be found in the Supporting Information. For P-silicene, in principle, there is no favorable site to adsorb the molecular gas. The interaction of NH_3 and CO with P-silicene is mostly of van der Waals type, whereas NO and NO_2 exhibit covalent chemisorption bonding. For doped devices, the gas molecules energetically prefer to be chemisorbed on the top of a B atom for B-silicene and chemisorbed on the top of a Si atom nearest to the N dopant for N-silicene. The binding energies of doped-silicene become larger than that of pristine, and the binding distances between the gases and doped-devices are shortened (see Table 1) as expected.

To better understand the binding strength of gas adsorption, we analyzed the charge density of three nanosensors, i.e., pristine and with the two dopants, as shown in Figure 2. The

Table 1. Calculated Binding Energy (E_b), Binding Distance (D),[a] and Charge Transfer from the Silicene to Molecules $\Delta Q(|e|)$

devices	gas	E_b (eV)	D (Å)	$\Delta Q(\lvert e\rvert)$
P-silicene	NO	−0.73	2.11	0.19
	NO_2	−1.30	1.77	0.37
	NH_3	−0.26	2.27	0.16
	CO	−0.10	3.24	−0.03
B-silicene	NO	−1.01	1.46	0.19
	NO_2	−3.02	1.50	0.08
	NH_3	−0.80	1.63	0.49
	CO	−1.19	1.51	0.32
N-silicene	NO	−1.95	1.87	0.01
	NO_2	−3.50	1.76	−0.06
	NH_3	−0.80	2.06	0.42
	CO	−0.99	1.88	0.20

[a]Binding distance (D) is defined as the shortest atom-to-atom distance between the molecule and silicene.

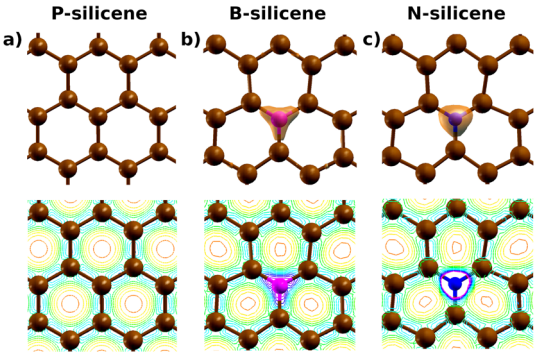

Figure 2. Charge density for (a) pristine silicene; (b) B-doped silicene, and (c) N-doped silicene. The plotted isosurface corresponds to a value of 0.08 $e \times \text{bohr}^{-3}$ for all panels.

pristine device was considered a neutral device, in which the charge density is equally distributed through the device. Although the doped nanodevices were also neutral, they had charge localization in the vicinity of each dopant that led to the conclusion that atoms had electron acceptor and donor characteristics for B and N dopants, respectively. We furthermore considered the electronegativity of all species involved in the devices. For B-silicene, the charge is concentrated close to B (it became slightly negative) and the three nearest-neighbor Si partially share this charge. The second device doped with N has higher charge accumulation close to N, compared to the former case, and the neighbor Si atoms become less charged. These facts are due to the electronegativity hierarchy of Si and dopant atoms; (N ≫ B ≳ Si). N has a tendency to attract electrons more strongly than B and Si. Figure 2 confirms this assumption that the charge was localized on the dopant for N-silicene and spread up the bonds for the B-silicene system.

The binding sites and molecular orientations of adsorbed gases on the nanosensor devices (Figure 1) needs to be discussed in more detail. For example, NO with an odd number of valence electrons has one unpaired electron on N atom which makes it highly reactive. As a result, NO always binds to the pristine silicene with N atom (see panel NO in center of Figure 1). As the second case in point, NH_3 has a tendency to bind to the pristine system with N, while the three H atoms

DOI: 10.1021/acs.jpcc.5b03635
J. Phys. Chem. C XXXX, XXX, XXX−XXX

point up. This is the simplest case because NH_3 has a lone pair on a N atom. The interesting case is for N-silicene, both dopant and gas have N atoms with the same electronegativity. Consequently, the NH_3 prefer binding with one Si atom close to a N atom (see Figure 1). Comparing the adsorption of NH_3, NO, and NO_2 on P-silicene with previously reported results,[36] our calculated binding energies are seen to differ in general by less than approximately 18%, however, the disagreement is larger for NH_3. When compared to the binding energy and the charge transfer of NH_3 on P-silicene in ref 15, our results agree quite well; there is a difference of 28.8% for binding energy and the value of charge transfer is exactly the same. The variation in results could be due to the difference of localized basis and plane-wave basis as well as the difference of dispersion correction. Additionally, our results are found to be in good agreement with a previous DFT study[35] except for the cases of physisorbed gases, i.e., CO and NH_3. The binding energy difference between those results and ours for NH_3 amounts to almost 60%. This large discrepancy stems from the inclusion of the long-range van der Waals (vdW) interactions in our present work. Furthermore, we systematically optimized the adsorption geometry of each gas molecule considering various possible molecular orientations and adsorption sites as a starting point for each relaxation (see the Supporting Information). Overall, we find qualitatively good agreement with previous studies for the most stable configuration of the adsorbate on P-silicene. However, when the device is doped, the gas prefers binding to the devices with a C atom. Finally, for NO_2 on P- and N-silicene devices, a covalent bond is formed between the Si atom and O atom due to the existence of an unpaired electron on one of the O atoms. For B-silicene, it is more energetically favorable that NO_2 binds to the system with its N atom. This results from the coordinate covalent bond in which an electron pair on the N atom enter into a vacant p-orbital on the B atom.

Possibility of Silicene Device as a Gas Sensor. Two of the most important challenges to build a good commercial sensor are the ability to detect different harmful gases (selectivity) and to improve the ability to sense some gas molecules (sensitivity). Experimentally, one of the most important parameters for sensing a gas is usually a variation in resistance or conductance, known as sensitivity. This property can be defined as $S\ (\%) = \frac{|G - G_0|}{G_0}$, where G and G_0 are the zero bias conductance for nanosensor with and without gas, respectively. Here, the conductance was simply calculated as $G = G_0 T(E_F)$, where $G_0 = 2e^2/h$ is the quantum conductance, e is the charge of the electron and h is Planck's constant.

The transmittance $T(E)$ of the P-, B-, and N-silicene devices is presented in Figure 3, parts a–c, respectively. Obviously, the gas adsorption significantly affects the $T(E)$ of the three devices. For example, the adsorption of NO and NO_2 on P-silicene results in a remarkable decrease of the $T(E)$, whereas for CO and NH_3 the changes are not very pronounced. Additionally, the results indicate that doping either B or N atoms into silicene improves the detection of CO and NH_3, compared to that of P-silicene. Without the presence of gas, the $T(E)$ of doped-silicene was lower than that of the P-silicene (as depicted by the black dashed line in Figure 3). The $T(E)$ of B-silicene was lower than that of N-silicene. It was shown that the

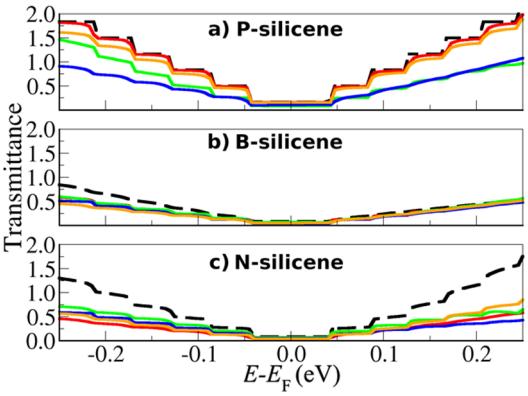

Figure 3. Transmittance as a function of energy E, where the Fermi energy (E_F) is set at zero, is shown for (a) P-silicene; (b) B-silicene, and (c) N-silicene. Red, green, orange, and blue lines represent the transmittance for CO, NO, NH_3, and NO_2 adsorbed on the devices, respectively, while black dashed lines represent that of the reference system (P-, B-, and N-silicene devices without gas).

gas adsorption on the B-silicene device affected the $T(E)$, but not as strongly as for N-silicene.

Figure 4a presents the sensitivity as a function of binding energy of the three devices (P-, B-, and N-silicene) for NO, NO_2, NH_3, and CO gas molecules. In order to evaluate whether silicene and doped silicene can be good gas nanosensors, we should have both high and distinct sensitivities when the sensor is exposed to different gases. Another important aspect is about how long the gas can stay on the device. This is the residence time (τ) and it is proportional to $\approx \exp\left(\frac{-E_b}{k_B T}\right)$, where E_b is binding energy, k_B is the Boltzmann constant and T is temperature. We expect small binding energies to lead to fast desorption of gases from the devices. Analyzing Figure 4a, we found that the binding energies were generally less than 2 eV. The only exception occurred for NO_2 on the doped-devices ($E_b > 3$ eV). Turning our focus to each device, we observed that the P-silicene device (see Figure 4b) has binding energies ranging from −0.1 to −1.3 eV and their respective sensitivities were strongly dependent on gas molecules. The sensitivity of the P-silicene device increased linearly with increasing binding energy. The sensitivities were found to follow an ascending order; i.e., CO < NH_3 < NO < NO_2. However, CO and NH_3 have low sensitivity. Spin-polarized calculations were also performed, but the resulting energy differences are smaller than the thermal fluctuations at the envisioned operating temperature of the sensor, namely room temperature ($k_B T \approx 0.025$ eV). In a test, we found that the transmittance for each channel (up and down) exhibits only minor quantitative differences which do not affect our conclusions. For these reasons, spin polarization effects were neglected in our study.

Next, we will address how to improve the sensitivity of these gases. As can be seen in Figure 4a, by the introduction of dopant atoms, N-silicene (diamond shape) and B-silicene (square shape) exhibited higher binding energies and subsequently sensitivity. This is especially true for CO and NH_3 (see Figure 4, parts c and d). Better sensitivity was obtained due to increased binding energies (see Table 1). Interestingly, CO molecules can distinguish p-type and n-type doping of silicene (see Figure 4c). This contradicts the findings of a previous study of a graphene-based gas sensor.[7] The CO on N-doped silicene showed a sensitivity around 2 orders of

DOI: 10.1021/acs.jpcc.5b03635
J. Phys. Chem. C XXXX, XXX, XXX−XXX

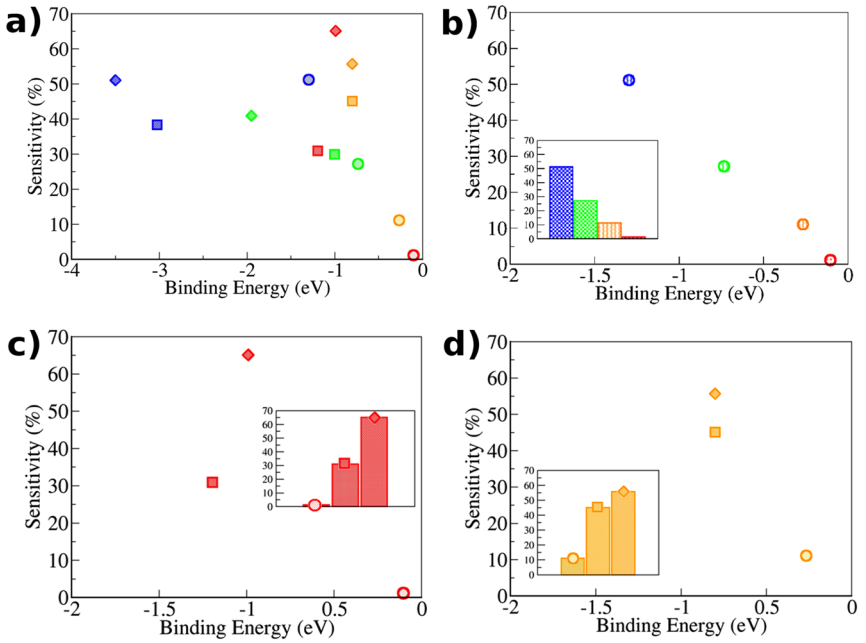

Figure 4. (a) Sensitivity versus binding energy for NO (green), NO_2 (blue), NH_3 (orange) and CO (red) gas molecules on P-silicene (circle), B-silicene (square) and N-silicene (diamond) devices, respectively; (b) the four gas species on P-siliene (the inset shows the sensitivity comparison for P-silicene); (c) CO on three devices and (d) NH_3 on three devices. The insets of parts c and d are the sensitivity comparison for one gas on the three different devices.

magnitude higher than that of CO on B-doped silicene. To explain why the sensitivity increased substantially for these molecular gases, the charge transfer of these systems will be investigated.

The transport properties of silicene devices relate to the change in local charge distribution around the B and N impurity atoms as a consequence of the charge transfer from gas molecules adsorbed on silicene. To visualize the charge transfer of NH_3 and CO adsorbed on the devices, we calculate the charge density difference $\Delta\rho(\vec{r}) = \rho_{device+gas}(\vec{r}) - (\rho_{device}(\vec{r}) + \rho_{gas}(\vec{r}))$, as presented in Figure 5.

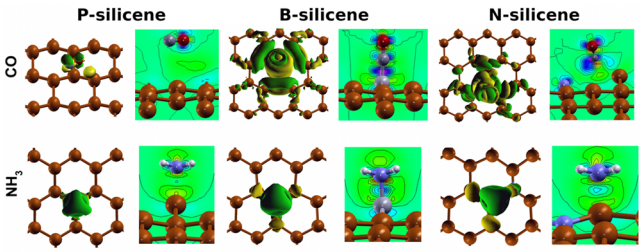

Figure 5. Charge density difference for CO (upper) and NH_3 (lower panel) on P-, B-, and N-silicene devices for each type of nanosensor. Isosurfaces are plotted for isovalues of 0.0004 (0.002) $e \times \text{bohr}^{-3}$ for CO (NH_3) alongside contour plots. For the isosurface plots, green color represents negative charge density difference while yellow corresponds to a positive change in charge density.

The contour plot of $\Delta\rho$ illustrates the charge accumulation/depletion in the system, i.e., we can quantitatively describe the idea of the charge transfer. For doped silicene, there is charge accumulation indicating the hybridization of orbitals at the nanosensor surface in which NH_3 and CO is adsorbed (see Figure 5). Such orbital hybridization is absent for physisorption of the gases on P-silicene. In other words, the charge-transfer capability increases with the increasing bonding charge densities.

Furthermore, we investigated the electron charge transfer using the Mulliken population analysis (see Table 1). It is notable that the positive charge transfer occurred from the gas molecules to the silicene. As discussed above, our results reveal the difference in charge redistribution of three nanosensors (see Figure 2). For B-silicene, as shown in Table 1, all gases examined in the current study act as donors. They donate charges to the device, resulting from the vacant p-orbital on the B atom. A large amount of charge transfer is obtained, especially for NH_3, which is electron-donating molecule. For N-silicene, the electron-rich gas molecules prefer to adsorb on the top of one positively charged Si close to N (see Figure 1). A negative charge transfer value as observed only for NO_2 due to its strong electron-withdrawing capabilities.

A few important aspects should also be discussed. The first is the influence of substrates on gas sensing performance. According to the experimental studies, for all the cases, silicene was synthesized on top of some substrates.[20−22,24] A very recent study[35] elaborated the effect of Ag(111) substrate on the electronic structures of gas molecules on silicene, indicating a slight increase in adsorption energies and charge transfer. We expected that the conductance could be changed due to the influence of different substrates, changing the sensitivity, but the interaction between silicene should not substantially change the overall trend with this additional component. The second point is about the experimental challenge to control the doping in silicene. Recent experimental studies reported on potassium adsorption in silicene,[47] inducing n-type doping. Additionally, a theoretical study also showed the stability of B/N substituted doping into silicene.[48] Therefore, if reactive centers can be created as we have shown, their gas sensing performance will be improved enormously. In addition, there remain many challenging problems. For instance, a recent study[49] demonstrated the dissociative adsorption of molecules (H_2, O_2, CO,

DOI: 10.1021/acs.jpcc.5b03635
J. Phys. Chem. C XXXX, XXX, XXX−XXX

H_2O, and OH) on defect sites in graphene and silicene. In our study, these molecules remain intact on silicene, but certain molecules may dissociate due to increased chemical reactivity at the defect sites as it has been reported previously.[49]

CONCLUSIONS

In conclusion, we investigated the capability of silicene-based devices for sensing chemical gases in terms of sensitivity and selectivity. We employed first-principles electronic structure calculations based on density functional theory formalism. For adsorption of NO, NO_2, NH_3, and CO on pristine (P-), B-doped, or N-doped silicene, we determine the adsorption configurations, binding energies, charge transfer and change in the electronic transport properties. Our results reveal that P-silicene can detect NO and NO_2 gas molecules with high sensitivity. However, this is limited to CO and NH_3 due to weak van der Waals interaction between those gases and P-silicene. By doping P-silicene with either B or N atoms, enhanced binding and charge transfer of all studied gases on the nanosensor were achieved, resulting in an increased sensitivity toward NH_3 and CO detection. However, doped-silicene strongly bound to NO and NO_2 is not presumably suitable for practical gas sensor devices. On the basis of our results, we can conclude that by doping with different impurities, one can create a silicene device that is able to detect different gas species with high sensitively and selectivity.

ASSOCIATED CONTENT

Supporting Information

Starting configurations for P-silicene and B/N-doped silicene. The Supporting Information is available free of charge on the ACS Publications website at DOI: 10.1021/acs.jpcc.5b03635.

AUTHOR INFORMATION

Corresponding Author

*(J.P.) E-mail: jariyanee.prasongkit@npu.ac.th. Telephone: +66 42 587 306 Fax: +66 42 587 306.

Present Address

[⊥]Departamento de Química, Instituto Tecnológico de Aeronáutica, São José dos Campos, São Paulo, Brazil.

Notes

The authors declare no competing financial interest.

ACKNOWLEDGMENTS

J.P. gratefully acknowledges financial support from the Thailand Research Fund (MRG5680186). R.G.A. and S.C were both supported by scholarships from the Carl Tryggers Foundation. R.H.S. would like to thank the Swedish Research Council (VR, Grant No. 621-2009-3628) for financing his position, and the Gender Equality Fund from the Department of Physics and Astronomy at Uppsala University for inviting J.P. for a research visit there. R.A. would also like to acknowledge the Swedish Research Council (VR, Grant No. 621-2012-4379) and Swedish Energy Agency. V.A. would like to thank the Nanotechnology Center (NANOTEC), NSTDA, Ministry of Science and Technology, Thailand, through its program of Centers of Excellence Network. The Swedish National Infrastructure for Computing (SNIC), the Uppsala Multidisciplinary Center for Advanced Computational Science (UPPMAX), and Versatus HPC provided computing time for this project.

REFERENCES

(1) Schedin, F.; Geim, A. K.; Morozov, S. V.; Hill, E. W.; Blake, P.; Katsnelson, M. I.; Novoselov, K. S. Detection of Individual Gas Molecules Adsorbed on Graphene. *Nat. Mater.* **2007**, *6*, 652−655.

(2) He, Q.; Wu, S.; Yin, Z.; Zhang, H. Graphene -Based Electronic Sensors. *Chem. Sci.* **2012**, *3*, 1764−1772.

(3) Fowler, J. D.; Allen, M. J.; Tung, V. C.; Yang, Y.; Kaner, R. B.; Weiller, B. H. Practical Chemical Sensors from Chemically Derived Graphene. *ACS Nano* **2009**, *3*, 301−306.

(4) Some, S.; Xu, Y.; Kim, Y.; Yoon, Y.; Qin, H.; Kulkarni, A.; Kim, T.; Lee, H. Highly Sensitive and Selective Gas Sensor Using Hydrophilic and Hydrophobic Graphenes. *Sci. Rep.* **2013**, *3*, 1868.

(5) Deng, S.; Tjoa, V.; Fan, H. M.; Tan, H. R.; Sayle, D. C.; Olivo, M.; Mhaisalkar, S.; Wei, J.; Sow, C. H. Reduced Graphene Oxide Conjugated Cu_2O Nanowire Mesocrystals for High-Performance NO_2 Gas Sensor. *J. Am. Chem. Soc.* **2012**, *134*, 4905−4917.

(6) Leenaerts, O.; Partoens, B.; Peeters, F. Adsorption of H_2O, NH_3, CO, NO_2, and NO on Graphene: A First-Principles Study. *Phys. Rev. B: Condens. Matter Mater. Phys.* **2008**, *77*, 125416.

(7) Zhang, Y.-H.; Chen, Y.-B.; Zhou, K.-G.; Liu, C.-H.; Zeng, J.; Zhang, H.-L.; Peng, Y. Improving Gas Sensing Properties of Graphene by Introducing Dopants and Defects: A First-Principles Study. *Nanotechnology* **2009**, *20*, 185504.

(8) Dai, J.; Yuan, J.; Giannozzi, P. Gas Adsorption on Graphene Doped with B, N, Al, and S: A Theoretical Study. *Appl. Phys. Lett.* **2009**, *95*, 232105.

(9) Cahangirov, S.; Topsakal, M.; Aktürk, E.; Şahin, H.; Ciraci, S. Two- and One-Dimensional Honeycomb Structures of Silicon and Germanium. *Phys. Rev. Lett.* **2009**, *102*, 236804.

(10) Jose, D.; Datta, A. Structures and Chemical Properties of Silicene: Unlike Graphene. *Acc. Chem. Res.* **2014**, *47*, 593−602.

(11) Lin, X.; Ni, J. Much Stronger Binding of Metal Adatoms to Silicene than to Graphene: A First-Principles Study. *Phys. Rev. B: Condens. Matter Mater. Phys.* **2012**, *86*, 075440.

(12) Vogt, P.; De Padova, P.; Quaresima, C.; Avila, J.; Frantzeskakis, E.; Asensio, M. C.; Resta, A.; Ealet, B.; Le Lay, G. Silicene: Compelling Experimental Evidence for Graphenelike Two-Dimensional Silicon. *Phys. Rev. Lett.* **2012**, *108*, 155501.

(13) Houssa, M.; van den Broek, B.; Scalise, E.; Pourtois, G.; Afanas'ev, V. V.; Stesmans, A. An electric field tunable energy band gap at silicene/(0001) ZnS interfaces. *Phys. Chem. Chem. Phys.* **2013**, *15*, 3702−3705.

(14) Drummond, N. D.; Zólyomi, V.; Fal'ko, V. I. Electrically Tunable Band Gap in Silicene. *Phys. Rev. B: Condens. Matter Mater. Phys.* **2012**, *85*, 075423.

(15) Kaloni, T. P.; Schreckenbach, G.; Freund, M. S. Large Enhancement and Tunable Band Gap in Silicene by Small Organic Molecule Adsorption. *J. Phys. Chem. C* **2014**, *118*, 23361−23367.

(16) Denis, P. A. Stacked Functionalized Silicene: A Powerful System to Adjust the Electronic Structure of Silicene. *Phys. Chem. Chem. Phys.* **2015**, *17*, 5393−5402.

(17) Kaloni, T. P.; Singh, N.; Schwingenschlögl, U. Prediction of a Quantum Anomalous Hall State in Co-Decorated Silicene. *Phys. Rev. B: Condens. Matter Mater. Phys.* **2014**, *89*, 035409.

(18) Houssa, M.; Pourtois, G.; Heyns, M. M.; Afanas'ev, V. V.; Stesmans, A. Electronic Properties of Silicene: Insights from First-Principles Modelling. *ECS Trans.* **2010**, *33*, 185−193.

(19) Lazar, P.; Karlický, F.; Jurečka, P.; Kocman, M.; Otyepková, E.; Šafářová, K.; Otyepka, M. *J. Am. Chem. Soc.* **2013**, *135*, 6372−6377.

(20) Feng, B.; Ding, Z.; Meng, S.; Yao, Y.; He, X.; Cheng, P.; Chen, L.; Wu, K. Evidence of Silicene in Honeycomb Structures of Silicon on Ag(111). *Nano Lett.* **2012**, *12*, 3507−3511.

(21) Vogt, P.; De Padova, P.; Quaresima, C.; Avila, J.; Frantzeskakis, E.; Asensio, M. C.; Resta, A.; Ealet, B.; Le Lay, G. Silicene: Compelling Experimental Evidence for Graphenelike Two-Dimensional Silicon. *Phys. Rev. Lett.* **2012**, *108*, 155501.

(22) Rachid Tchalala, M.; Enriquez, H.; Mayne, A. J.; Kara, A.; Roth, S.; Silly, M. G.; Bendounan, A.; Sirotti, F.; Greber, T.; Aufray, B.; et al.

DOI: 10.1021/acs.jpcc.5b03635
J. Phys. Chem. C XXXX, XXX, XXX−XXX

Formation of One-Dimensional Self-Assembled Silicon Nanoribbons on Au(110)-(21). *Appl. Phys. Lett.* **2013**, *102*, 083107.
(23) Fleurence, A.; Friedlein, R.; Ozaki, T.; Kawai, H.; Wang, Y.; Yamada-Takamura, Y. Experimental Evidence for Epitaxial Silicene on Diboride Thin Films. *Phys. Rev. Lett.* **2012**, *108*, 245501.
(24) Meng, L.; Wang, Y.; Zhang, L.; Du, S.; Wu, R.; Li, L.; Zhang, Y.; Li, G.; Zhou, H.; Hofer, W. A.; et al. Buckled Silicene Formation on Ir(111). *Nano Lett.* **2013**, *13*, 685−690.
(25) Tsai, W.-F.; Huang, C.-Y.; Chang, T.-R.; Lin, H.; Jeng, H.-T.; Bansil, A. Gated silicene as a tunable source of nearly 100% spin-polarized electrons. *Nat. Commun.* **2013**, *4*, 1500.
(26) Xu, C.; Luo, G.; Liu, Q.; Zheng, J.; Zhang, Z.; Nagase, S.; Gao, Z.; Lu, J. Giant Magnetoresistance in Silicene Nanoribbons. *Nanoscale* **2012**, *4*, 3111−3117.
(27) Ni, Z.; Zhong, H.; Jiang, X.; Quhe, R.; Luo, G.; Wang, Y.; Ye, M.; Yang, J.; Shi, J.; Lu, J. Tunable Band Gap and Doping Type in Silicene by Surface Adsorption: Towards Tunneling Transistors. *Nanoscale* **2014**, *6*, 7609−7618.
(28) Liu, H.; Gao, J.; Zhao, J. Silicene on Substrates: A Way to Preserve or Tune Its Electronic Properties. *J. Phys. Chem. C* **2013**, *117*, 10353−10359.
(29) Ni, Z.; Liu, Q.; Tang, K.; Zheng, J.; Zhou, J.; Qin, R.; Gao, Z.; Yu, D.; Lu, J. Tunable Bandgap in Silicene and Germanene. *Nano Lett.* **2012**, *12*, 113−118.
(30) Tao, L.; Cinquanta, E.; Chiappe, D.; Grazianetti, C.; Fanciulli, M.; Dubey, M.; Molle, A.; Akinwande, D. Silicene Field-Effect Transistors Operating at Room Temperature. *Nat. Nanotechnol.* **2015**, *10*, 227−231.
(31) Jose, D.; Datta, A. Structures and Electronic Properties of Silicene Clusters: A Promising Material for FET and Hydrogen Storage. *Phys. Chem. Chem. Phys.* **2011**, *13*, 7304−7311.
(32) Hussain, T.; Chakraborty, S.; Ahuja, R. Metal-Functionalized Silicene for Efficient Hydrogen Storage. *ChemPhysChem* **2013**, *14*, 3463−3466.
(33) Sadeghi, H.; Bailey, S.; Lambert, C. J. Silicene-Based DNA Nucleobase Sensing. *Appl. Phys. Lett.* **2014**, *104*, 103104.
(34) Amorim, R. G.; Scheicher, R. H. Silicene as a New Potential DNA Sequencing Device. *Nanotechnology* **2015**, *26*, 154002.
(35) Feng, J.-w.; Liu, Y.-j.; Wang, H.-x.; Cai, Q.-h.; Wang, X.-z. Gas Adsorption on Silicene: A Theoretical Study. *Comput. Mater. Sci.* **2014**, *87*, 218−226.
(36) Hu, W.; Xia, N.; Wu, X.; Li, Z.; Yang, J. Silicene as a Highly Sensitive Molecule Sensor for NH_3, NO and NO_2. *Phys. Chem. Chem. Phys.* **2014**, *16*, 6957−6962.
(37) Hohenberg, P.; Kohn, W. Inhomogeneous Electron Gas. *Phys. Rev.* **1964**, *155*, 864−870.
(38) Kohn, W.; Sham, L. Self-Consistent Equations Including Exchange and Correlation Effects. *Phys. Rev.* **1965**, *385*, 1133−1138.
(39) Soler, M.; Artacho, E.; Gale, J. D.; Garcia, A.; Junquera, J.; Ordejon, P.; Sánchez-Portal, D. The SIESTA Method for Ab Initio Order- N Materials. *J. Phys.: Condens. Matter* **2002**, *14*, 2745−2779.
(40) Dion, M.; Rydberg, H.; Schröder, E.; Langreth, D. C.; Lundqvist, B. I. Van der Waals Density Functional for General Geometries. *Phys. Rev. Lett.* **2004**, *92*, 246401.
(41) Román-Pérez, G.; Soler, J. Efficient Implementation of a van der Waals Density Functional: Application to Double-Wall Carbon Nanotubes. *Phys. Rev. Lett.* **2009**, *103*, 096102.
(42) Perdew, J. P.; Burke, K.; Ernzerhof, M. Generalized Gradient Approximation Made Simple. *Phys. Rev. Lett.* **1996**, *77*, 3865−3868.
(43) Troullier, N. Efficient Pseudopotentials for Plane-Wave Calculations. *Phys. Rev. B: Condens. Matter Mater. Phys.* **1991**, *43*, 1993−2006.
(44) Kresse, G.; Furthmüller, J. Efficient Iterative Schemes for Ab Initio Total-Energy Calculations Using a Plane-Wave Basis Set. *Phys. Rev. B: Condens. Matter Mater. Phys.* **1996**, *54*, 11169.
(45) Brandbyge, M.; Mozos, J.-L.; Ordejón, P.; Taylor, J.; Stokbro, K. Density-Functional Method for Nonequilibrium Electron Transport. *Phys. Rev. B: Condens. Matter Mater. Phys.* **2002**, *65*, 165401.
(46) Rocha, A.; García-Suárez, V.; Bailey, S.; Lambert, C.; Ferrer, J.; Sanvito, S. Spin and Molecular Electronics in Atomically Generated Orbital Landscapes. *Phys. Rev. B: Condens. Matter Mater. Phys.* **2006**, *73*, 085414.
(47) Friedlein, R.; Fleurence, A.; Sadowski, J. T.; Yamada-Takamura, Y. Tuning of Silicene-Substrate Interactions with Potassium Adsorption. *Appl. Phys. Lett.* **2013**, *102*, 221603.
(48) Sivek, J.; Şahin, H.; Partoens, B.; Peeters, F. M. Adsorption and Absorption of Boron, Nitrogen, Aluminum, and Phosphorus on Silicene: Stability and Electronic and Phonon Properties. *Phys. Rev. B: Condens. Matter Mater. Phys.* **2013**, *87*, 085444.
(49) Gürel, H. H.; Özçelik, V. O.; Ciraci, S. Dissociative Adsorption of Molecules on Graphene and Silicene. *J. Phys. Chem. C* **2014**, *118*, 27574−27582.

DOI: 10.1021/acs.jpcc.5b03635
J. Phys. Chem. C XXXX, XXX, XXX−XXX

Supplementary Material for: Highly sensitive and selective gas detection based on silicene

Jariyanee Prasongkit,[*,†,‡] Rodrigo G. Amorim,[¶] Sudip Chakraborty,[¶] Rajeev Ahuja,[¶,§] Ralph H. Scheicher,[¶] and Vittaya Amornkitbamrung[‖,‡]

Division of Physics, Faculty of Science, Nakhon Phanom University, Nakhon Phanom, 48000, Thailand, Nanotec-KKU Center of Excellence on Advanced Nanomaterials for Energy Production and Storage, Khon Kaen 40002, Thailand., Division of Materials Theory, Department of Physics and Astronomy, Box 516, Uppsala University, SE-751 20 Uppsala, Sweden, Applied Materials Physics, Department of Materials Science and Engineering, Royal Institute of Technology (KTH), SE-100 44 Stockholm, Sweden, and Department of Physics, Faculty of Science, Khon Kaen University, 123 Mittraphab Road, Khon Kaen 40002, Thailand

E-mail: jariyanee.prasongkit@npu.ac.th

Unit cell and supercell

Silicene has a hexagonal lattice with two atoms per unit cell (A and B) as is shown in Figure S1-a. However, is also possible define an unit cell with four atoms and parallepiped shape (see Figure S1-b), in which the lattice is characterized by three lattice vectors L_x, L_y and L_z. In particular both unit cells are equivalent, but as we are interested in transport properties through the device

[*]To whom correspondence should be addressed
[†]Nakhon Phanom University
[‡]Nanotec-KKU Center of Excellence on Advanced Nanomaterials for Energy Production and Storage
[¶]Uppsala University
[§]Royal Institute of Technology
[‖]Khon Kaen University

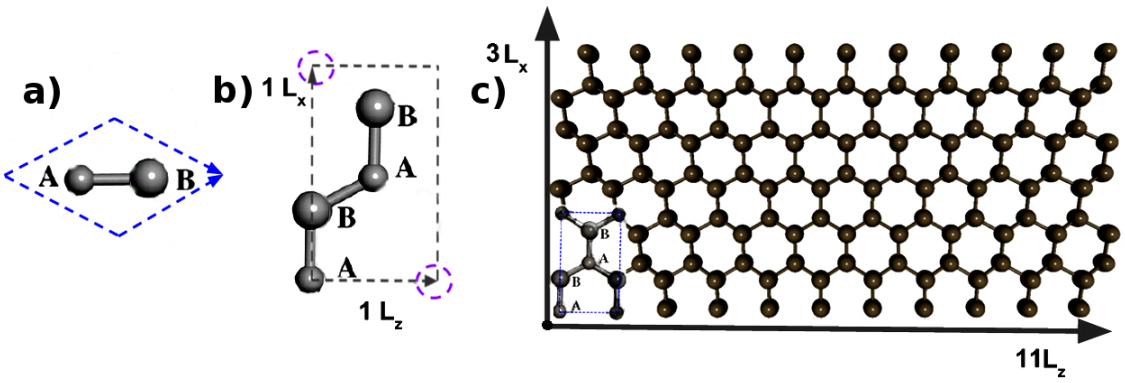

Figure S1: a) Hexagonal 2D lattice with two atoms per unit cell for silicene; b) A parallelepiped unit cell with four atoms per unit cell and (c) supercell used in relaxations and also transport calculation.

in certain direction, the parallelepiped unit cell fits better for this application. In all calculation were employed a supercell using a parellepiped unit cell with $3L_x \times L_y \times 11L_z$ *and 132 atoms as is shown in Figure S1-c. The referred supercell has* $20.57\text{Å} \times 15\text{Å} \times 43.54\text{Å}$.

Geometry relaxation

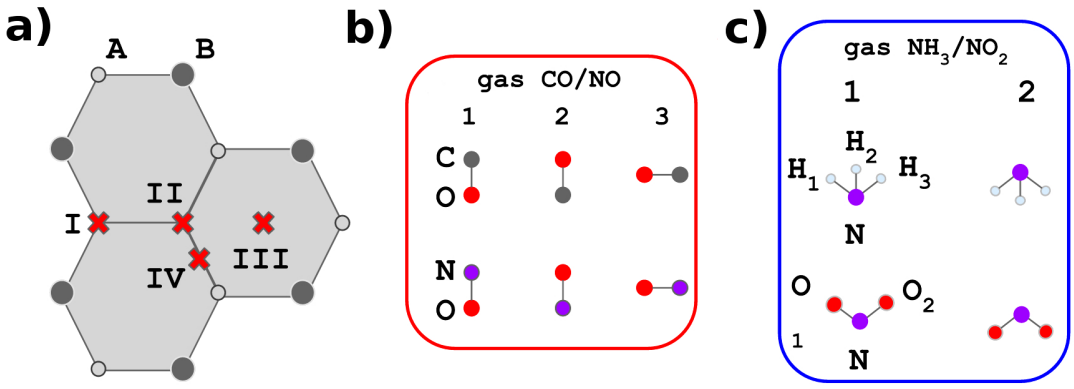

Figure S2: (a) Possible adsorption sites of gases on the hexagonal lattice of P-silicene: (I) hill, (II) valley, (III) bridge, and (IV) hollow sites. Different molecular orientations were examined for (b) CO and NO (diatomic gas molecules) with three possible orientations and (c) NH_3 and NO_2 (tri- and tetra-atomic gas molecules) with two initial orientations.

Figure S2-(a) shows four possible adsorption sites of gases on the P-silicene. They are referred to as the (I) hill, (II) valley, (III) bridge, and (IV) hollow sites. For these positions, different

molecular orientations were examined. For diatomic gases (CO and NO), we investigated three possible orientations. Their molecular axis was oriented parallel and perpendicular (with the O pointing up and down) with respect to the silicene surface. For tri- and tetra- atomic gases (NH_3 and NO_2), two orientations were tested, i.e., one with the N atom pointing to the surface and the other with the N atom pointing away from the surface. These can be seen in Figure S2-(b,c).

For P-silicene, twelve starting configurations for CO and NO (diatomic gases) and eight for NO_2 and NH_3 (tri-/tetra- atomic gases) were considered. Note that the starting configuration was not the final one. We sometimes see energy degenerated structures with very small binding energy differences. CO has two degenerate adsorption configurations, i.e., III-3 and IV-3. NO exhibits two most stable configurations, i.e., II-2 and III-2. NH_3 presents two degenerate adsorption configurations, i.e, IV-1 and II-1. The most stable configurations including its binding energy and binding distance are presented in the main manuscript.

For doped-silicene, we examined only the gas adsorption above the dopants and their nearest neighbors since these adsorption sites are the most active. As shown in the main manuscript, we observed that different gases exhibit distinct configurations for each doped-silicene device. CO and NO (diatomic gases) binding with the doped-silicene at the C and N atom, respectively. They were tilted with respect to the surface for N- silicene, but aligned perpendicularly for B-silicene. NH_3 bonds to the silicene with its N atom for both doped-devices. NO_2 bonds to B-silicene with its N atom (B-N bond) and to N-silicene with an O atom (Si–O bond).